Marine and Petroleum Geology 138 (2022) 105530

Contents lists available at ScienceDirect

Marine and Petroleum Geology

journal homepage: www.elsevier.com/locate/marpetgeo

Arc-parallel shears in collisional orogens: Global review and paleostress analyses from the NW Lesser Himalayan Sequence (Garhwal region, Uttarakhand, India)

Tuhin Biswas [a], Narayan Bose [b], Dripta Dutta [c], Soumyajit Mukherjee [a,*]

[a] Department of Earth Sciences, Indian Institute of Technology Bombay, Powai, Mumbai, 400 076, Maharashtra, India
[b] Department of Geology & Geophysics, Indian Institute of Technology Kharagpur, Kharagpur 721 302, West Bengal, India
[c] Experimental Rock Deformation Laboratory, Department of Earth Sciences, Indian Institute of Technology Kanpur, 208 016, Uttar Pradesh, India

ARTICLE INFO

Keywords:
Brittle shear
Paleostress
Stress regime
NW Lesser himalayan sequence

ABSTRACT

Interest in hydrocarbon exploration from the Lesser Himalayan Sequence (LHS) has recently been revived amongst the petroleum geoscientists. Understanding the paleostress regime and the deformation mechanism are the two important steps to understand the structural geology of any (petroliferous) terrains. Arc-parallel shear is an integral deformation process in orogeny. The scale of such deformation features can range from micro-mm up to regional-scale. Unlike arc-orogen-perpendicular shear, different driving forces can produce arc-parallel shears. We review these mechanisms/theories from several orogens including the Himalaya, and compile 44 locations worldwide with arc-parallel shear. Due to continuous crustal shortening by the India-Eurasia collision, the squeezed rock mass at the plate interface has been building the Himalayan mountain chain. In addition, the rock mass also escapes laterally along the orogenic trend. Tectonic stress-field governs this mass flow. Field study and microstructural analysis in the northwest LHS (India) reveals arc-parallel brittle and ductile shear movement. Y- and P- brittle shear planes, and the S- and C- ductile shear planes reveal the following shears documented on the ~ NW-SE trending natural rock selections: (i) top-to-NW up, (ii) top-to-SE up, (iii) top-to-NW down, and (iv) top-to-SE down. Our paleostress analysis indicates top-to-SE down and top-to-NW down shears occurred due to stretching along ~131°–311° (D_{ext}), whereas top-to-SE up and top-to-NW up shear fabric originated due to shortening along ~133.5°–313.5° (D_{compr}). Previous authors considered that the arc-parallel extension generated ~15-5 Ma due to vertical thinning of the Himalaya. The NE-trending Delhi-Haridwar Ridge below the LHS plausibly acted as a barrier to the flowing mass, and piled up the rock mass in the form of NW-SE/arc-parallel compression. The NW-SE compression can be correlated with the D_3 of Hintersberger et al. (2011) during ~ 4–7 Ma.

1. Introduction

"… although many of the key concepts in the structural geology of fold and thrust belts have earlier origins in other orogens, the impetus has come from the desire to exploit geological resources that reside in the subsurface." - Hammerstein et al. (2020).

Structural geology and tectonic models of fold and thrust belts/collisional orogens primarily control the spatial distribution of the hydrocarbon reserves (Cooper, 2007). Small and complicated structures in such terrains hold the possibility of hydrocarbon (review in Hammerstein et al., 2020). In 1960s the Oil and Natural Gas Commission (ONGC) tried to explore hydrocarbon in the Himalaya, and got a limited success. Independent and infrequent geoscientific studies in the Himalaya continued in this direction (e.g., Rao, 1986; Mukherjee and Chakrabarti, 1996). Palaeontological studies on Ediacara led Tewari (2012) to speculate hydrocarbon source rock from the Neo-Proterozoic terrain of the Lesser Himalayan Sequence (LHS), Garhwal Indian Himalaya. In fact, Neoproterozoic-Cambrian hydrocarbon reserves have been gaining attention worldwide. For example, Proterozoic rocks in the Jammu region (NW Himalaya, India) are presently under study for hydrocarbon (Hakhoo et al., 2016).

Despite pessimist scientific views that fold and thrust belts/

* Corresponding author.
E-mail addresses: tbtuhin24@gmail.com (T. Biswas), narayan.bghs@gmail.com (N. Bose), dripta.dutta@gmail.com (D. Dutta), soumyajitm@gmail.com, smukherjee@iitb.ac.in (S. Mukherjee).

https://doi.org/10.1016/j.marpetgeo.2022.105530
Received 5 March 2021; Received in revised form 1 January 2022; Accepted 3 January 2022
Available online 19 January 2022

collisional orogens such as the Himalaya in general has a poor chance of hydrocarbon exploration (Goffey et al., 2010), or the postulation that some specific part of the LHS can be non-productive (Mishra and Mukhopadhyay, 2012), ONGC has been targeting the Krol unit of rocks from the LHS, NW Himalaya, India (Bhattacharya, Internet Reference; Bose and Mukherjee, 2020). The Krol and Tal units of the LHS are potential reservoir of moderate quality (reviewed in Table 1 of Mishra and Mukhopadhyay, 2012). Besides, the Blaini unit in the LHS have a good hydrocarbon potential (review in Craig et al., 2018). LHS rocks in Pakistan (Riaz et al., 2019) and in Nepal (Neupane et al., 2020) also have quite good potential and active hydrocarbon (shale gas, liquid hydrocarbon etc.) producing fields (e.g., Pakistan: Jhelum riverine system; Nepal: oil and gas seepages in Dailekh).

Several research papers on paleostress analysis elucidate the role of such a study in deciphering the petroleum geology of (sedimentary) terrains. To refer a few, Sippel et al. (2010) reconstructed the paleostress field in the petroliferous Oslo graben (Norway) and linked them with the rift-related local igneous activities. Kulikowski and Amrouch (2018) used 3D seismic data to analyze paleostress from the Cooper–Eromanga Basin (Australia) that has implication in understanding the hydrocarbon migration pathways (also see Zeng et al., 2010 for a similar study). Scheiber and Viola (2018) analyzed paleostress from fractures in the country rocks at the northern Bømlo islands (Norway). They separated deformation phases and linked those with the Caledonian orogeny and rifting. A similar approach of separating out deformation phases by performing paleostress studies was conducted by Ju et al. (2017) from the Sichuan basin (China). Kleinspehn et al. (1989) utilized paleostress study in deciphering the subsidence history of the petroliferous Central Basin of Spitsbergen, which is an important input in the basin's petroleum geology.

Around 55 Ma back, the northward advancing Indian plate made a continent-continent collision with the Eurasian plate (Klootwijk et al., 1992; Yin, 2006; Copley et al., 2010) and started initiating the classic Cenozoic Himalayan mountain chain. The orogen commonly comprises of compressional (Yin, 2006) and intriguing extensional structures (Kellett et al., 2019). These can be well understood at arc-parallel natural (sub-)vertical rock sections (Godin et al., 2006). Not only the shortened rock materials at the interface of Indian and the Eurasian plate led to orogenesis, rock materials also flowed/sheared laterally (Molnar and Tapponier, 1975). This is well understood for the Tibetan region as well where materials extended E-W in addition to significant N–S shortening (GPS velocity study, Zhang et al., 2004). However, in the Himalaya ~ N–S shortening also dominates in terms of in-sequence and out-of-sequence thrusting, that verges both towards foreland (towards ~ S) and hinterland (towards ~ N) (e.g., Ni and Barazangi, 1984; Mukherjee, 2015; Mukherjee, 2015; Bose and Mukherjee, 2019a, b; Ghosh and Mukherjee, 2021).

Arc-parallel extension and compression have been reported from worldwide (review in Fig. 1), including the Himalaya (review in Fig. 2). Twelve possibilities of geneses are complied for such deformation (Table 1).

Orogensis has been deduced mostly based on the study of regional thrusts [e.g., Gansser, 1964; Burchfiel et al., 1992; Vannay et al., 2004 in case of the Himalaya] in which the small-scale brittle deformation signatures have sometimes been missed. However, these (sub)meter-scale faults and ductile shear zones have great potential to provide detail deformation phases of different segments of the mountain. For example, the Karakorum fault situated between the Tibetan Plateau and the Himalaya slipped >1000 km to accommodate the crustal shortening (Peltzer and Tapponnier, 1988). Interestingly, study of small-scale brittle structures from the southern part of the Karakorum Fault tightly constrained the slip magnitude of this fault to be only 65 km (e.g., Murphy et al., 2002) to < 400 km (e.g., Lacassin et al., 2004).

In this article, we document shear senses parallel to the regional orogenic trend in the NW Lesser Himalaya Sequence (Uttarakhand state, India) to understand the deformation behaviour parallel to the orogen.

Table 1
Globally reported arc-parallel extension and compression, compiled in this study.

Sl no.	Model name	Example	References
Arc-parallel extension			
1.	Gravitational Collapse	Yilgarn Craton, Australia[a] Samnagawa metamorphic Complex[b] Alpine orogen[c] Himalayan orogen[d]	a. Davis and Maidens (2003) b. Takeshita and Yagi (2004) c. Jolivet et al. (1999) d. Dalmayrac and Molnar (1981); Molnar et al. (1983), Royden et al., 1997 Molnar and Lyon-Caent (1989) Ratschbacher et al. (1994)
2.	Radial Thrusting and Expansion	GIlbraltar Arc in Alboran Sea[a] Himalayan orogen[b]	a. Platt and Vissers (1989); Martínez-Martínez and Azañón (1997) and references therein b. Treloar and Coward (1991); Murphy and Copeland (2005); Murphy et al. (2009); Hintersberger et al. (2011); Seeber and Armbruster (1984); Armijo et al. (1986)
3.	Oroclinal Bending	Himalayan orogen[a] Central Anatolian Plateau[b] New England orogen[c] NW and Central Iberia[d] Median Tectonic Zone of New Zealand[e] South Carpathians[f]	a. Ratschbacher et al. (1994); Kapp and Yin (2001); Robinson et al. (2007) b. Özsayin and Dirik (2011) c. Shaanan et al. (2015) d. Catalán et al. (2014) e. Bradshaw et al. (1996) f. Schmid et al. (1998)
4.	Removal of Mantle	Himalayan orogen[a] Trans-Hudson orogen[b] Western Anatolia[c] Southern Tibet[d] Zargosmountains[e] Delamerian-Ross fold belt in Australia[f]	a. England and Houseman (1989) b. Ansdell et al. (1995) c. Dilek and Altunkaynak (2007) d. Hoke et al. (2000); Miller et al. (1999) e. Mouthereau et al. (2012) f. Turner et al. (1996)
5.	Oblique Convergence	Himalayan orogen[a] South-Central CanandianCordillera[b], Western Alps[c], Variscides of France[d] NE Venezuela[e]	a. McCaffrey and Nabelek (1998); Styron et al. (2011) a-d. Ellis and Watkinson (1987) e. Avé Lallemant and Guth (1990)
6.	Dome Extrusion	Eastern Alps[a] Betics in southeast Spain[b] NW Iberia in Spain[c] The Menderes massif in southwest Turkey[d] Variscan French Massif[e] Himalayan orogen[f]	a. Ratschbacher et al. (1989); Frisch et al. (2000) b. Martínez-Díaz and Hernández-Enrile (2004) c. Viruete (1999) d. Hetzel et al. (1995) e. Faure (1995) f. Thiede et al. (2006); Aoya et al. (2005)
7.	Rigid Plate indentor	Alps mountain belt[a] Aegean arc[b] Himalaya orogen[c]	a. Ratschbacher et al. (1989); Bonini et al. (1999); Robl and Stüwe (2005), b. Martinod et al. (2000) c. Kapp and Guynn (2004)
8.			

(continued on next page)

Table 1 (*continued*)

Sl no.	Model name	Example	References
	Basement influence on cover	Southern Urals[a] Himalaya[b] Zagros Mountain[c] NW Taiwan[c] N Apennines[c]	a. Brown et al. (1999) b. Godin et al. (2019) c. Lacombe and Bellahsen (2016)
9.	Mass accumulation and stored energy dissipation	Himalayan orogen[a]	a. Hodges et al. (2001)
Arc-Orogen parallel compression			
10.	Oblique Convergence	Central America[a] Northern Chile Forearc/ Andes[b] Central Andes[c]	a. McCaffey (1996) b. McCaffey (1996); Allemendinger et al. (2005) c. Boutelier and Oncken (2010)
11.	Plate Rotation	Northern Apennines[a]	a. Carosi et al. (2004) and references therein; Viti et al. (2004)
12.	Abrupt termination of lateral massflow	Himalayan orogen[a]	a. Seeber and Pêcher (1998)

We attempt to correlate arc-parallel shear with the existing models. We present meso-and micro-scale evidences of arc-parallel shears and perform paleostress analysis on brittle shears. Various models explaining origin of extensional and compressional deformation parallel to the arc are compared. However, lack of cross-cut relation restrict our understanding of their relative timing. This work is important since arc-parallel shears can trigger landslides and earthquakes.

2. Arc-parallel rock movement

2.1. Arc-parallel extension, the concept

Extensional structures parallel to the orogen trend has been recorded profusely (Fig. 1) but lacks unified theory for their genesis. From over-thickening of the crust to extension within the orogen marks a remarkable shift in the stress regime. Shape/geometry of an orogen, gravity driven mass flow, change in mantle flow along the collisional margin, angular convergence between two colliding plates, dome extrusion, approaching plate acting as rigid component, basement cover relationship etc. can govern the arc-parallel extension. To explain these, the following models have been postulated with different driving forces.

(a) Gravitational collapse(mechanism: Fig. 3 i; global occurrence: Fig. 1)

Collisional margin induces a significant change in gravitational potential energy during lithospheric deformation. A gravity-driven ductile flow compensates the generated anomalous potential energy producing extensional structures parallel to the ductile flow direction (Rey et al., 2001). The mechanism depends on horizontal compressional stresses, basal shear stress between the two plate boundaries, change in potential energy, strength of the adjoining materials and the crustal strength (Rey et al., 2001 and references therein).

(b) Radial thrusting and expansion (mechanism: Fig. 3 ii; global occurrence: Fig. 1)

Converging plate acting as an indentor after collision gives rise to radially outward thrust system dying out at the orogen margin. To preserve such an expanding shape of the collisional margin, local extensional and strike-slip features (Seeber and Armbuster, 1984; Murphy and Copeland, 2005) develop synchronous with the radial listric thrusts. Extension is presumably maximum at the central part of the collisional margin and dies out towards the flanks. Platt and &Vissers (1989) additionally suggested that due to additional emplacement of asthenosphere mantle under the collisional margin, surface elevates and eventually the orogen grows.

(c) Oroclinal bending (mechanism: Fig. 3 iii; global occurrence: Fig. 1)

Orogens bent around a vertical axis of rotation are called oroclines (Carey, 1955). Progressive oroclines (Johnston et al., 2013) are characterized by small-scale structures, thin-skinned tectonics, a single stress-field generating the thrust belt as well as the orogenic bending. Secondary oroclines (Johnston et al., 2013) are plate-scale. Here orogeny involves lithospheric mantle along with the crust and orogenic bending. A compression near-perpendicular to the original compressive stress-field develops. In secondary oroclines, lithospheric mantle plays a vital role in modifying surface features. The theory is popular in many orogens and explains their extensional structures.

(d) Removal of Mantle(mechanism: Fig. 3 iv; global occurrence: Fig. 1)

England and Houseman (1989) numerically modelled collision-induced overthickened lithosphere where the hot asthenosphere replaces the colder and denser mantle lithosphere. This involves "convectional thinning" of the lithosphere that elevates the topography. A differential stress between the elevated topography and its low-lying surroundings may lead to extensions locally in a regionally compressive tectonic setting giving rise to arc-parallel extension.

(e) Oblique convergence (mechanism: Fig. 3 v; global occurrence: Fig. 1)

When a plate approaches another plate obliquely, the line of action of stress normal to the plate boundary results in compression within the plate, whereas the arc-parallel component results in strike-slip faults, extensional faults/shear zones within the fore-arc region (Avé Lallemant and Guth, 1990). Inter-plate earthquake data along the convergent margin can confirm this oblique convergence based on the angle between the shortening slip directions and the direction of convergence (McCaffrey, 1996). Oblique convergence is characterized by an arc--parallel extension with meso-scale cylindrical isoclinal folds and stretching lineations sub-parallel to the orogenic trend (Ellis and Watkinson, 1987).

(f) Domal extrusion (mechanism: Fig. 3 vi; global occurrence: Fig. 1)

Convergence between two plates over-thickens, heats up and weakens the continental crust (e.g., England and Richardson, 1977). Plate-scale deformation melts crust partially (e.g., Nelson et al., 1996). Further convergence develops extensional and strike-slip faults, and exhumes high-grade rocks at the domal core (e.g., Lee at el., 2000; Lee et al., 2004; Dutta and Mukherjee, 2021). These exhumed metamorphic domes weakens crust further and accommodates more intrusion at shallow crustal level during the ongoing collision leading to localized arc-parallel extension (Aoya et al., 2005).

(g) Rigid plate indenters (mechanism: Fig. 3 vii; global occurrence: Fig. 1)

A rigid subducting basement, upon collision with another plate, results in initially gently-dipping thrusts followed by arc-parallel extension in the form of a "continental escape" in response to crustal thickening (Ratschbacher et al., 1989). The collisional features are

governed by the geometry and the dip of the approaching rigid plate. Bonini et al. (1999) studied the progressively changing geometry of a rigid indentor after collision and coined the term "effective indentor". In this model, the normal and the thrust faults predate the arc-parallel strike slip faulting (Martinod et al., 2000).

(h) Basement Influence on cover (mechanism: Fig. 3 viii; global occurrence: Fig. 1)

Reactivation of pre-existing structures in the basement is common in collisional margins and plays a crucial role in orogenesis (Brown et al., 1999 and references therein). Lacombe and Bellahsen (2016) pointed out the requirement of thick-skinned tectonics to understand crustal deformation on a collisional boundary. Basement highs in the present-day foreland regions placed at a high-angle to the collisional margin shortens the crust leading to arc-parallel extensions on the cover rocks.

2.2. Arc-parallel compression-the concept

Arc-parallel compression has been recorded only from a few orogens globally (Fig. 1). Schellart et al. (2004) doubted compression parallel to the orogen based on the large-scale elastic behaviour of the lithosphere and the retaliate behaviour of the lithospheres surrounding the particular orogen. Arc-parallel compression appears to be area-specific and can be due to rotation of the colliding plates, oblique convergence and existence of barrier to prevent lateral mass-flow. Models for arc-parallel compression are presented below.

(a) Oblique Convergence (mechanism: Fig. 4 i; global occurrence: Fig. 1):

When a low-dipping subducting plate attains a high-angle of obliquity at collisional margin in between two plates, friction between the colliding plates increases temporally to effectively produce arc-parallel

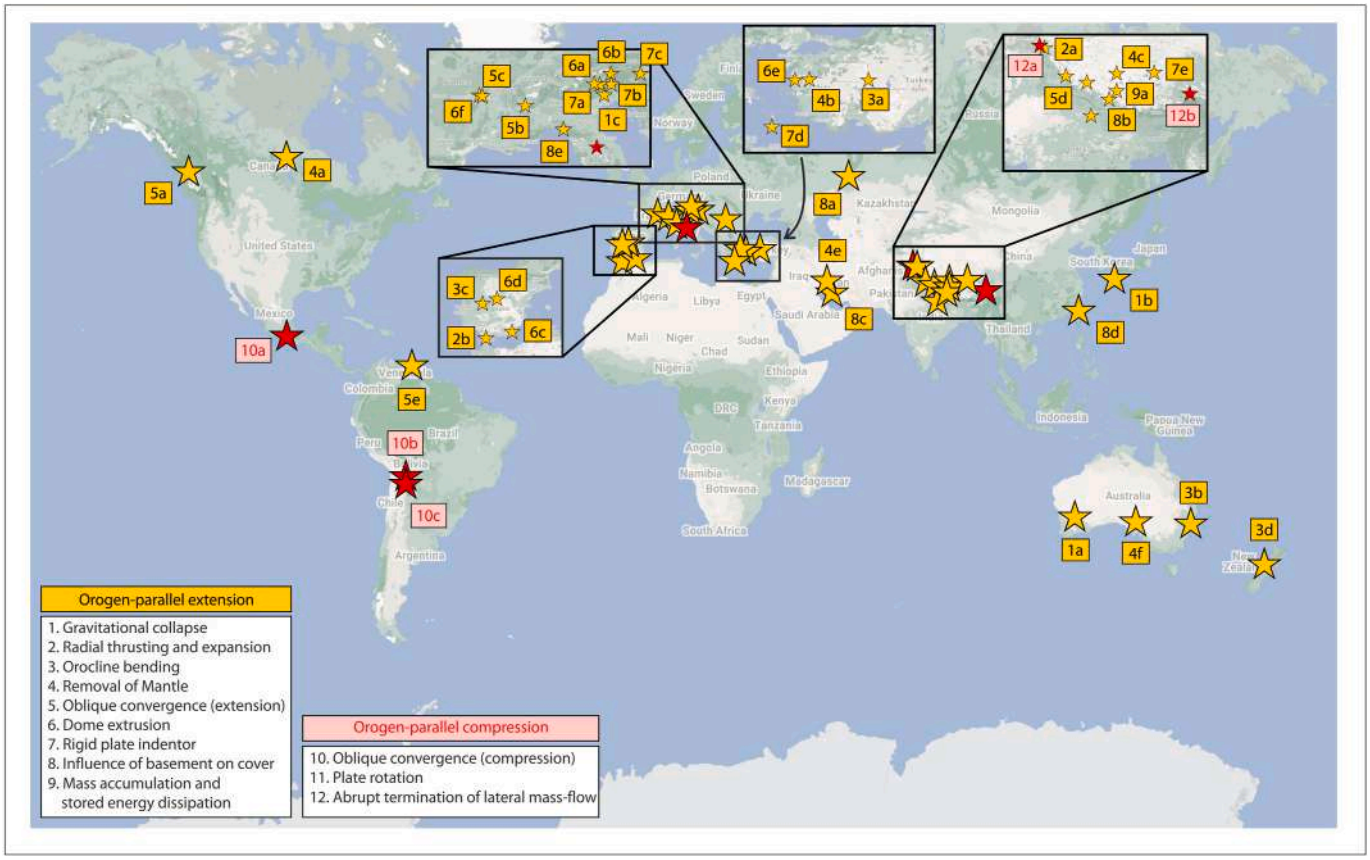

Fig. 1. Global distribution of arc-parallel deformation reported in the literature, compiled in this study. See Table 1 for related information. Map is constructed using Google My Maps, (accessed on 12-Oct-2020). The numbers represent existing models enlisted in the legend at bottom left corner. 1a: Yilgarn Craton, Australia- Davis and Maidens (2003); 1b: Samnagawa metamorphic Complex, Japan- Takeshita and Yagi (2004); 1c: Alpine orogen- Jolivet et al. (1999); 2a: Himalayan orogen- Treloar and Coward (1991); 2b: Gilbraltar Arc in Alboran Sea- Platt and Vissers (1989), Martínez-Martínez and Azañón (1997) and references therein; 3a: Central Anatolian Plateau- Özsayin and Dirik (2011); 3b: New England orogen-Shaanan et al. (2015); 3c: NW and Central Iberia- Catalán et al. (2014); 3d: Median Tectonic Zone of New Zealand- Bradshaw et al. (1996); 3c: South Carpathians- Schmid et al. (1998); 4a: Trans-Hudson orogen- Ansdell et al. (1995); 4b: Western Anatolia- Dilek and Altunkaynak (2007); 4c: Southern Tibet- Hoke et al. (2000); 4d: Southern Tibet- Miller et al. (1999); 4e: Zargos mountains- Mouthereau et al. (2012); 4f: Delamerian- Ross fold belt in Australia- Turner et al. (1996); 5a: South-Central Canandian Cordillera- Ellis and Watkinson (1987); 5b: Western Alps- Ellis and Watkinson (1987); 5c: Variscides of France- Ellis and Watkinson (1987); 5d: Himalayan orogen- Ellis and Watkinson (1987); 5e: NE Venezuela- Avé Lallemant and Guth (1990); 6a: Eastern Alps- Ratschbacher et al. (1989); 6b: Eastern Alps- Frisch et al. (2000); 6c: Betics in southeast Spain-Martínez-Díaz and Hernández-Enrile (2004); 6d: NW Iberia in Spain- Viruete (1999); 6e: The Menderes massif in southwest Turkey- Hetzel et al. (1995); 6f: Variscan French Massif- Faure (1995); 7a: Alps- Ratschbacher et al. (1989); 7b: Alps- Bonini et al. (1999); 7c: Alps- Robl and Stüwe (2005); 7d: Aegean arc- Martinod et al. (2000); 7e: Himalayan orogen- Kapp and Guyn (2004); 8a: Southern Urals- Brown et al. (1999); 8b: Himalaya- Godin et al.(2019); 8c: Zagros Mountain- Lacombe and Bellahsen (2016); 8d: NW Taiwan- Lacombe and Bellahsen (2016); 8e: N Apennines- Lacombe and Bellahsen (2016); 9a: Himalayan orogen- Hodges et al. (2001); 10a: Central America- McCaffey (1996); 10b: Northern Chile Forearc/Andes- Allemendinger et al. (2005); 10c: Central Andes- Boutelier and Oncken (2010); 11a: Northern Apennines- Carosi et al. (2004) and references therein; 11b: Northern Apennines- Viti et al. (2004); 12a: Nanga Parbat, Himalaya- Seeber and Pêcher (1998); 12b: Namcha Barwa syntaxis, Himalaya- Seeber and Pêcher (1998).

compression (Boutelier and Oncken, 2010). Plates may curve as a response to stress, and this plays a vital role to develop such compression (Boutelier and Oncken, 2010).

(b) Plate rotation (mechanism: Fig. 4 ii; global occurrence: Fig. 1)

If a microplate is involved in a collisional margin, rotation and reorientation of such plate accompanied by continuous collision produces arc-parallel compression (Boccaletti and Sani, 1998; Viti et al., 2004). A small plate rotating under compression must have high mechanical strength and remain in no contact with surrounding plates (Viti et al., 2004) (Fig. 3iii). Wide-scale bend, strike-slip fault and small-scale lateral escape of materials are characteristics of arc-parallel compression (Mantovani et al., 1997a, 2002; Gelabert et al., 2002; Mantovani, 2004).

(c) Abrupt termination of lateral mass flow (mechanism: Fig. 4 iii; global occurrence: Fig. 1)

Collisional boundaries are characterized by overthickening followed by lateral escape of such mass to dissipate the accumulated energy. If these laterally escaping mass encounters a sudden dead end/stress buttress [regional structural boundary, e.g., Nanga Parbat syntaxis in Himalayan orogen, Seeber and Pêcher (1998)], the mass tends to accumulate against such termini. If the termini are ~ perpendicular to orogen, arc-parallel compression will be the outcome (Seeber and Pêcher, 1998).

3. Arc-parallel shear in himalaya

Arc-parallel shear from the arcuate Himalayan chain have been recorded by several workers from Tethyan-, Higher-, Lesser- and the Siwalik Himalaya (Fig. 2).

3.1. Arc-parallel extension in the Himalaya-Tibet system

(a) Gravitational collapse (Fig. 3 i for mechanism; Himalayan occurrence: Fig. 2)

Higher elevations are prone to gravitational collapse, and as compression continues material escapes laterally in form of east–west extension in Himalaya-Tibet region (e.g. Molnar and Tapponier, 1975, 1978; Tapponnier and Molnar, 1976; Tapponnier et al., 1982; Valli et al., 2007, 2008).

(b) Radial thrusting and expansion (Fig. 3 ii for mechanism; Himalayan occurrence: Fig. 2)

The radial expansion theory is a step further from the radial thrusting (Section 2.1.b) in case of the Himalaya, where the sequential development of the thrust faults viz., the Main Central Thrust (MCT, ~25–0.7 Ma; Godin et al., 2006, Larson et al., 2015 review in Martin, 2017; also see Montemagni et al., 2019, 2020; Iaccarino et al., 2020; Montemagni and Villa 2021), the Main Boundary Thrust (MBT, ~11–9 Ma; review in Godin et al., 2019) and the Main Frontal Thrust (MFT, < 2.5 Ma; review in Mukherjee, 2015), is accounted for. Due to its arcuate geometry, arc-parallel stretching in the Himalaya increases towards the foreland. However, given that the MCT is the oldest amongst the three major discontinuities, Murphy et al. (2009) identified that the Tethyan Himalaya and the Trans-Himalaya are the areas of maximum arc-parallel stretching followed by Higher Himalayan Crystallines (HHC), LHS and then the Siwalik Himalaya.

(c) Oroclinal bending (Fig. 3 iii for mechanism; Himalayan occurrence: Fig. 2)

The Karakorum Fault and Yadong-Gulu rift cover a large part of Tibetan N–S rift system (e.g., Klootwijk et al., 1985) The central part of the Himalaya and southern Tibet are the most affected regions due to the arcuate shape of the Himalayan arc. Opposite sense of shear (Dutta and

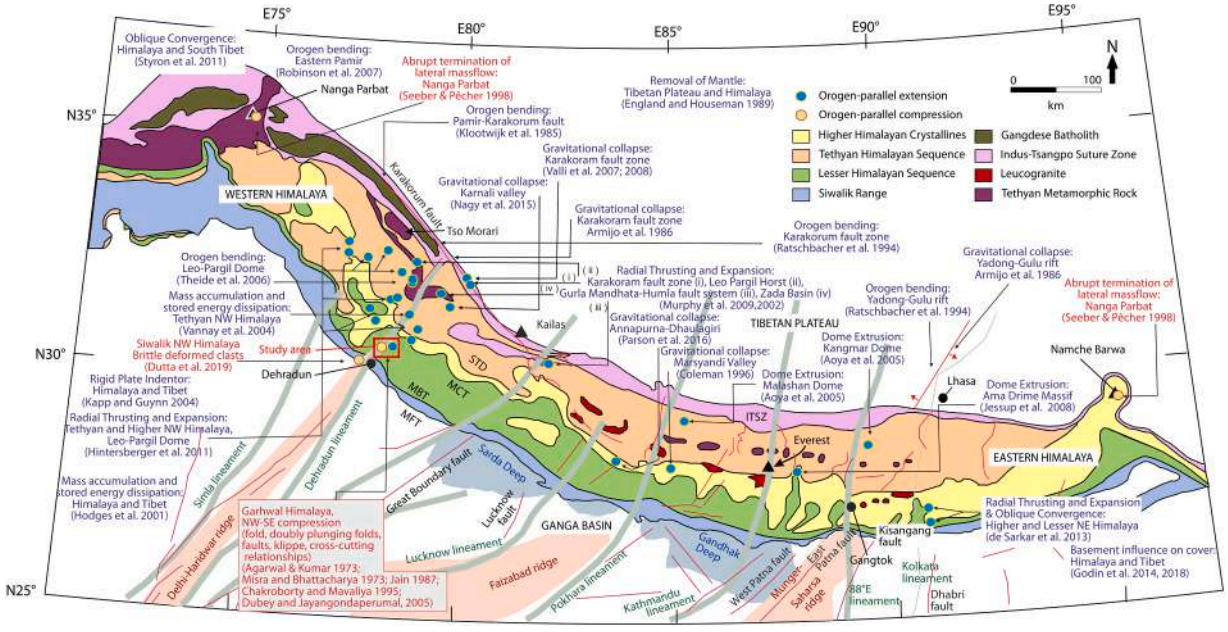

Fig. 2. Geologic map of the Himalaya (reproduced and modified from Zhang et al., 2015; Godin et al., 2019). Arc-parallel deformation recorded within the Himalayan belt by various authors is compiled on it in this work. Blue circle: arc-parallel extension; Yellow circle: arc-parallel compression. Major tectonic discontinuities: ITS: Indus Tsangpo Suture; STD: South Tibetan Detachment; MCT: Main Central Thrust; MBT: Main Boundary Thrust; MFT: Main Frontal Thrust. Light red shaded regions represent basement highs belonging to Indian plate. Thick grey lines: basement faults/lineaments belonging to the Indian plate based on Bouguer gravity data (Godin et al., 2019). Red lines: active fault planes belonging to India and Himalaya-Tibet system. Light blue: depression. Locations are represented by black circle and mountain peaks are by black triangles.

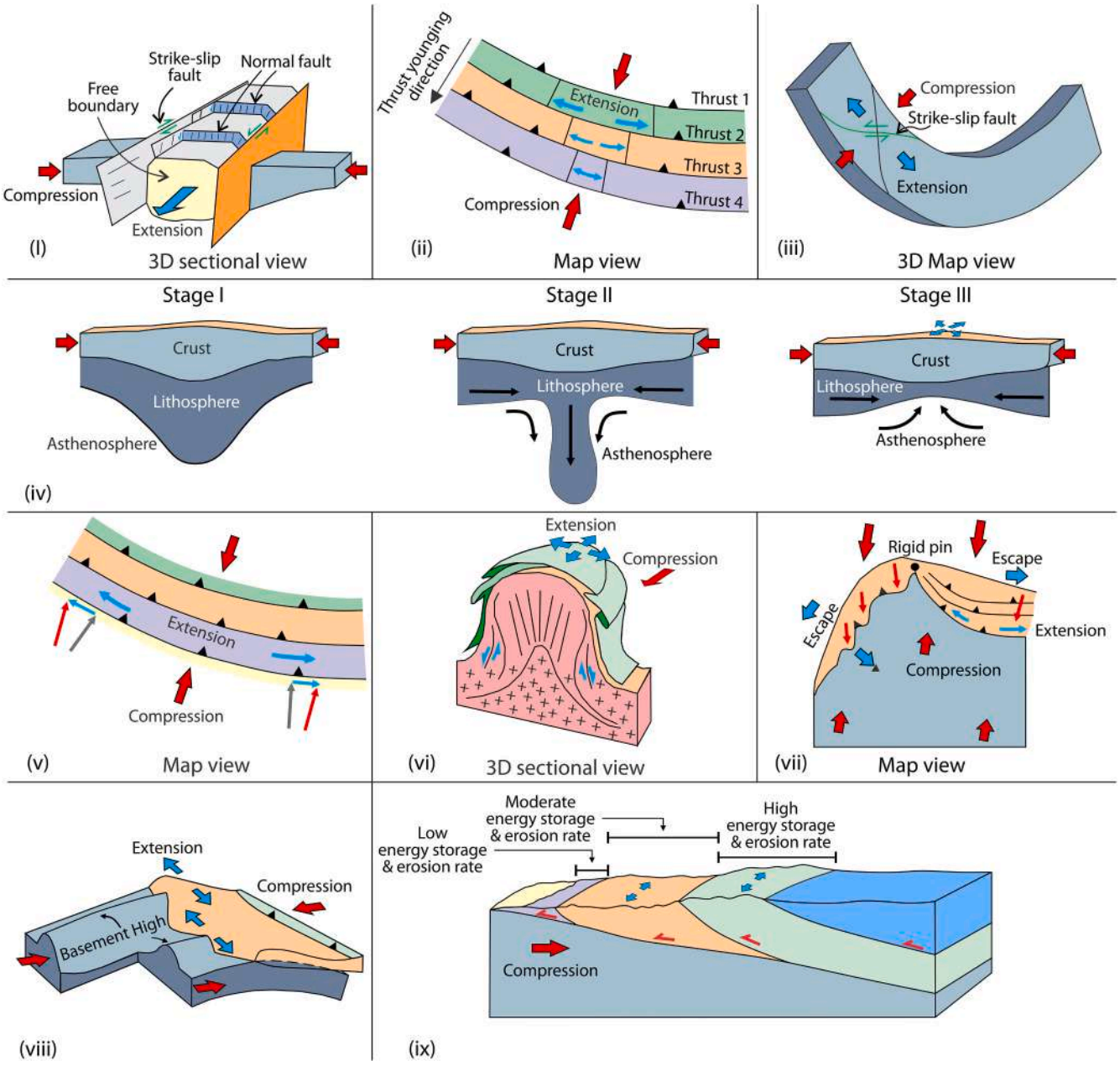

Fig. 3. Schematic existing arc-parallel extension models throughout the globe. Not to scale. Blue arrow: extension, Red arrow: compression, Green arrow: strike-slip. (i) Gravitational collapse model; (ii) radial thrusting and extension model; (iii) orocline bending model; (iv) removal of mantle model; (v) oblique convergence model; (vi) dome extrusion model; (vii) rigid plate indentor model; (viii) basement influence on cover model; (ix) mass accumulation and stored energy dissipation model.

Mukherjee, 2019) at the syntaxes indicates rotation of crustal blocks due to the orogenic bending.

(d) Removal of Mantle (Fig. 3 iv for mechanism; Himalayan occurrence: Fig. 2)

With the ongoing collision between the Indian and the Eurasian plate, an instability within mantle convection led to up-arching of the crustal surface (England and Houseman, 1989). Stress difference between the elevated surface and the surroundings produced arc-parallel extension in the Himalaya.

(e) Oblique convergence (Fig. 3 v for mechanism; Himalayan occurrence: Fig. 2)

No extensional structures developed in the central part of the Himalaya as the orientation of the interface between the Indian plate and Eurasian plate is ~ orthogonal to the direction of convergence. As per this model, Western Himalaya experiences westward material flow and the eastern Himalaya towards east due to the regional resultant stress orientation (Styron et al., 2011).

(f) Dome extrusion (Fig. 3 vi for mechanism; Himalayan occurrence: Fig. 2)

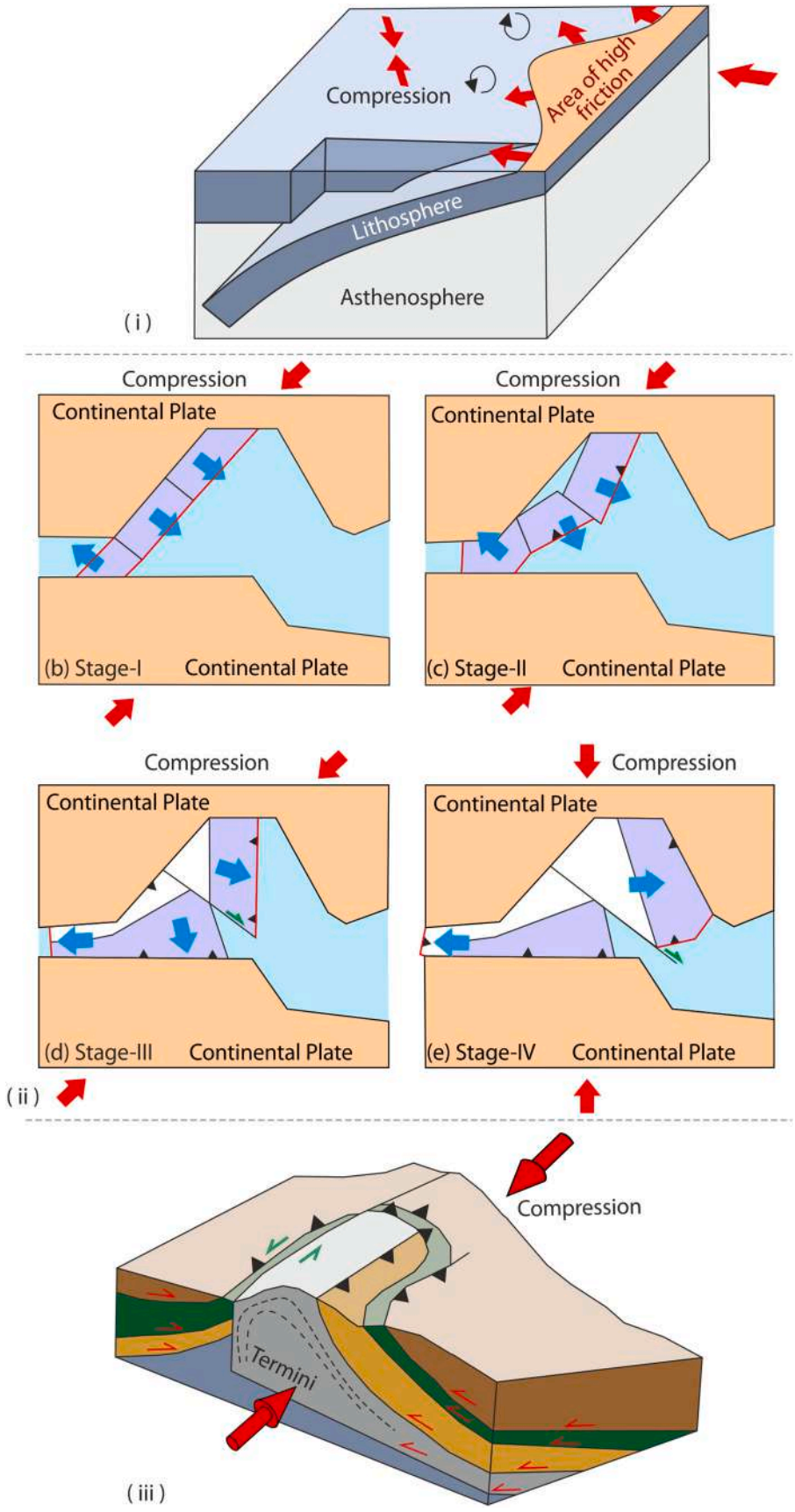

Fig. 4. Schematic diagrams of existing arc-parallel compression models throughout the globe. Not to scale. Red arrow represents compression, Blue arrow represents migration direction of the plate, green arrow represents strike-slip component. (i) Oblique convergence model; (ii) abrupt termination of lateral mass-flow model; (iii) plate-rotation model.

Table 2
Litho-tectonic succession of the LHS, compiled from Jain (1971); Jain et al. (1971); Agarwal and Kumar (1973); Jain and Varadaraj (1978); Kumar and Dhaundiyal (1979); Kumar and Dhaundiyal (1980); Azmi and Pancholi (1981); Sharma and Bhatt (1990); Thakur (1992); Bhatt (1996); Thakur and Kumar (1994); Kayal et al. (2002); Dubey and Jayangondaperumal (2005); Shekhar et al. (2006); Richards et al. (2005); Célérier et al. (2009); Valdiya (2010); Colleps et al. (2019). Note: a. Azmi and Pancholi (1981), b. Kumar and Dhaundiyal (1979), Kumar and Dhaundiyal (1980), c. Thakur (1992), d. 1220 Ma Thakur (1992), e. ~ 967 Ma (U/Pb dating of Galena mineralization; Thakur (1992)), f. Richards et al. (2005), g. ≤ 1.8 Ga Colleps et al. (2019)), h. ≤ 950 Ma Colleps et al. (2019)), i. ≤ 850 Ma Colleps et al. (2019), ≤770 Ma Colleps et al. (2019), k. 635-541 Ma Colleps et al. (2019).

Division of Lesser HimalayaSequence	Formation (Age)	Lithology/key features
MAIN BOUNDARY THRUST		
OUTER LESSER HIMALAYA	Tal Formation (Cambrian-Ordovician[a]/Jurrassic to Cretaceous[b]/Lower Cambrian[c])	Rich argillaceous matter of greenish-grey shale, black phosphorite-chert, bluish grey limestone altered with white purple quartzite deposited under shallow marine to inter tidal condition
	Krol Formation (Cambrian[a]/Permian to Triassic[b]/Early Cambrian[c]/Neoproterozoic[k])	Blue and black colored limestones altered with yellow-white, grey and buff colored quartzite and purple green, greyish green, black carbonaceous phyllite.
	Blaini Formation (Permo-Carboniferous[c]/Neoproterozoic[j])	Greenish-grey boulder conglomerate layers with sedimentary and low grade metamorphic provenance, along with carbonaceous as well as green-purple shale, grey siltstone, grey and purple dolomite, grey limestone, grey quartzites with non-fossiliferous glacio-marine origin.
	Nagthat Formation (Neoproterozoic[f,i])	Sericite schistose quartzites, purple, white and green quartz arenite, altered with shale and phyllites deposited under shallow tidal-sandbar zone
	BASUL THRUST AND AGLAR THRUST	
	Chadpur Formation/Dharmandal Group/Saryu Formation/ Dharasu Formation (Neoproterozoic[f,i])	Greyish green phyllite intercalated with grey and very fine metasiltstone and buff, grey metagraywacke, pinkish brown sublitharenitic quartzite occurring in massive habit.
TONS THRUST (SRINAGAR, NORTH ALMORA, DHARKOT, CHAIL 3 THRUST)		
INNER LESSER HIMALAYA	Rautgara Formation/Kotga Banali Group/Dunda Slate (Neo-Mesoproterozoic[h])	Muddy quartzite (subgreywacke to sublitharenite) altered with grey-greenish and purple color phyllite and green, purple, greyish black color slate. Ripple marks and mudcracks indicate delta deposit.
	Deoban Formation (Neoproterozoic[e,h])	Thick layers of stromatolite-cherty dolomites altered with quartzite and grey slates deposited under shallow marine condition.
	Mandhali Formation (Neoproterozoic[c]/Paleoproterozoic[h])	Blue and black colored limestones altered with yellow-white, grey and buff colored quartzite and purple green, greyish green, black carbonaceous phyllite.
	BERINAG THRUST (UTTARKASHI, DUNDA, SINGUNI, DHARASU THRUST)	
	Berinag Formation/Gamri Quartzite Dichli dolomite/ Pratapnagar Group/Garhwal Group (Mesoproterozoic[d]/ Paleoproterozoic[g])	Thick bedded of sugary sericitic quartzite, pinkish white to light green quartz arenite with little chlorite schist alteration. Oldest formation of LHS.
MUNSIARI THRUST (MCT_L)		
MCT ZONE SCHISTS		

Weakened collisional crust with continuous convergence exhumes the metamorphic core complexes within the Tethys Himalaya [e.g., Malashan Dome, Kangmar Domes etc. (Aoya et al., 2005)] on the surface, inducing lateral extension leading to arc-parallel extension.

(g) Rigid plate indenters (Fig. 3 vii for mechanism; Himalayan occurrence: Fig. 2)

The Indian plate as the rigid indenter collided with Eurasian plate and as a result arc-parallel extensional rift system developed. As per this theory, extension was restricted in the Central Himalaya (Kapp and Guynn, 2004).

(h) Basement Influence on cover (Fig. 3 viii for mechanism; occurrence in the Himalaya: Fig. 2)

Reactivation of pre-existing basement fault system within the Indian continent created lateral deformation zones within the Himalayan cover by affecting the geometry of the Main Himalayan Thrust (Godin et al., 2019). Bouguer gravity anomaly data reveals linear structural features along the Himalayan mountain range are deeply connected with the underplated basement faults (Godin et al., 2019).

(i) Mass accumulation and stored energy dissipation(Fig. 3 ix for mechanism; occurrence in the Himalaya: Fig. 2)

After Indo-Eurasian plate collision, the Himalaya and the Tibetan plateau continuously stored mass and therefore gravitational potential energy. A full grown orogen starts squandering the energy. At this time, domination in between accumulated energy and dissipated energy takes place. The stored energy is dissipated by the Himalayan front by reorganizing the structural and the erosion patterns. Such reorganization can be accompanied by seismicity. The reorganization can produce arc-parallel extension. In a full grown orogen squandering of energy dominates as the accumulation of energy fades out (Hodges et al., 2001).

3.2. *Arc-parallel compression in himalaya (Fig. 4 for mechanism; himalayan occurrence: Fig. 2)*

Arc-parallel compression in the Himalaya is deciphered from both the syntaxial boundaries. In east, the Namcha Barwa syntaxis (Wadia, 1931) and in the west the Nanga Parbat syntaxis (Madin et al., 1989) in form of antiforms (Seeber and Pêcher, 1998) and are coeval with the Himalayan regional compression (Burg et al., 1998).

In the NW Himalaya, arc-parallel compression has been well documented within the LHS (e.g., in form of fold, doubly plunging folds, faults, klippes, cross-cut relations; Agarwal and Kumar, 1973; Misra and Bhattacharya, 1973; Jain, 1987; Chakraborty and Mavaliya, 1995; Dubey and Jayangondaperumal, 2005) and within the Siwalik range in the Dehradun-Roorkee transect in terms of brittle deformed clasts (Dutta et al., 2019). To the authors' knowledge, arc-parallel compressional structures are absent in the Central and in the Eastern Himalaya (Fig. 2).

Major deformation within Himalaya pre-dating the Tertiary collision is not universally accepted. In the context of thick-skinned tectonics, pre-Himalayan deformation and its possible influence on Himalayan orogeny are to be considered profoundly. See Repository 1 for detail pre-Himalayan deformation (and metamorphism).

4. Timings of arc-parallel shear

After the Indian plate collided with the Eurasian plate, massive crustal thickening perpendicular to the orogen triggered lateral movement of mass manifested as arc-parallel extension between 15 and 5 Ma. For example, Nagy et al. (2015) reported extension ~15-13 Ma from the upper Karnali valley (Nepal) based on $^{40}Ar/^{39}Ar$ dating of white micas from the HHC. Zircon fission track dating reveals 12-11 Ma activation of arc-parallel extension from the HHC in the Sutlej valley, NW Indian Himalaya (Vannay et al., 2004). Inception of arc-parallel rock movement is presumed to be ~10 Ma within the HHC (cross-cut relation between the 12.5 Ma old Khula Kangri Granite and the South Tibetian Detachment: Edward and Harrison, 1997). Repository 2 presents arc-parallel shear from the Tibetan region.

5. Geology of the study area

The LHS is bounded by two active thrusts, the MBT to the south, and the MCT to the north. The MCT and the MBT separate the LHS from the HHC and the Siwalik Himalaya, respectively. The LHS is sub-divided by various major and minor longitudinal thrust sheets (Fig. 2, Table 2). Lack of ubiquitous fossil evidences, low-grade metamorphism (Miller et al., 2000) and brittle to brittle-ductile deformation render it difficult to compile a detailed and exhaustive stratigraphy. Nevertheless, previous workers (Valdiya, 1980; Srivastava and Mitra, 1994; Ahmad et al., 2000; DeCelles et al., 2001; Célérier et al., 2009; Richards et al., 2005) broadly divided the LHS into: (i) Outer Lesser Himalayan Sequence (OLHS), and (ii) Inner Lesser Himalayan Sequence (ILHS), based on the degree of deformation, age difference, strain rate and temperature. The north-dipping Tons Thrust (Célérier et al., 2009; Ahmad et al., 2000; Richards et al., 2005), separates the OLHS at south from the ILHS at north.

5.1. Lithologic & structural information

The entire LHS was deposited under a marine condition along with the Tethyan Himalayan Sequence (THS) within two separate basins (reviews in Thakur, 1992; Srivastava and Mitra, 1994). Fore-structures are foreland verging and dip towards the hinterland. Back-structures, on the other hand, dip and verge towards the foreland and hinterland, respectively. Fore and back structures are well documented and reported from the study area (Banerjee et al., 2019; Bose and Mukherjee, 2019a). Table 2 compiles the succession.

U–Pb isotopic signatures of detrital zircon suggest deformed LHS sediments' depositional ages, Paleoproterozoic to Neoproterozoic, are comparable with undeformed Vindhyan sediments within the Indian craton (McKenzie et al., 2011). The OLHS (succession in Table 2), underwent fault-propagation folding to create the Mussoorie Syncline and Garhwal Syncline (Fig. 1 in Kumar and Dhaundiyal, 1980) with the Tal Formation at the core (Shanker and Ganesan, 1973; Valdiya, 1978). Parallel to the synclinal axis is the northerly dipping Kathu-ki-Chail Thrust, which displaced the Tal Formation rocks locally creating klippes of the Precambrian Ramgarh Group and the Almora Group Crystallines (Fig. 5; Dubey and Jayangondaperumal, 2005). The Nagthat and the Chandpur Formations are separated by a north-dipping Aglar Thrust to the south, and a south-dipping Basul Thrust to the north (Fig. 5, Table 2; Jain, 1971). The Tons Thrust marks the contact between the OLHS and the ILHS (Célérier et al., 2009). It is a prominent back-thrust (Bose and Mukherjee, 2019a), which is also named as the Srinagar Thrust (Thakur and Kumar, 1994; Valdiya, 2010) and the North Almora Thrust (Agarwal and Kumar, 1973; Kayal et al., 2002), Dharkot Thrust, and the Chail 3 Thrust (Bhatt, 1996).

The ILHS is intensely folded and faulted (Valdiya, 1995). The Berinag Thrust (Dharasu Thrust/Singauni Thrust/Dunda Thrust/Uttarkashi Thrust, Jain, 1971; Agarwal and Kumar, 1973) is the most prominent discontinuity within the ILHS and is a folded thrust belt, separates the Rautgara-, Mandhani- and Deoban Formations with the Berinag Formation (Fig. 2, Table 2). The north-dipping Munsiari Thrust (Lower strand of the MCT: MCT_L) marks the upper limit of the LHS (Mukherjee, 2015) located near the Sainj village (also see Catlos et al., 2020; Montemagni et al., 2020). See Repository 3 for local structural detail.

Unlike the much well-studied orogen-perpendicular shear in ductile and brittle regimes (e.g., Mukhopadhyay and Mishra, 2005; Célérier et al., 2009; Agarwal et al., 2016; Bose and Mukherjee, 2019a,b), arc-parallel shear received much less attention from the LHS. In and around our study area, no absolute timing/constrain on arc-parallel compression and extension has been available.

5.2. Deformation timing

The S/SW-verging Main Boundary Thrust (MBT) marking the southernmost boundary of Lesser Himalaya Sequence was activated around 9–11 Ma (apatite fission track dating: Meigs et al., 1995; Thakur et al., 2014, $^{40}Ar/^{39}Ar$ dating of white micas: DeCelles et al., 2001; Robinson et al., 2006). The northern (and upper) and the southern (and the lower) strands of the Main Central Thrust, MCT_U and MCT_L, activated ~ 8–9 and ~ 5-4 Ma, respectively (Montemagni et al., 2020). Himalayan compression reactivated the Kathu-ki-Chail Thrust (Dubey, 2014), however, the exact timing remains unknown.

The once north-dipping Tons Thrust transported the autochthonous OLHS ~50–100 km south and rested it against the base of the ILHS (Célérier et al., 2009). Tons Thrust reactivated at ~14 Ma as a back-thrust (Patel et al., 2015; Agarwal et al., 2016).

The Berinag Thrust-fold belt responsible for klippes within ILHS sheared S/SW up (Bose and Mukherjee, 2019a). Mandal et al. (2016) predicted Berinag Thrust to be genetically equivalent to the Munsiari Thrust (Ramgarh-Munsiari Thrust). However, Singh et al. (2012) suggested a younger age (apatite fission track date of 0.3 ± 0.1 to 0.9 ± 0.2 Ma) for the Berinag Thrust than that of the Munsiari Thrust (1.7 ± 0.4 Ma, 1.8 ± 0.2 Ma and 2.3 ± 0.3 Ma; apatite fission track) and correlated with reactivation of duplex within the ILHS.

$^{40}Ar/^{39}Ar$ dating and zircon fission track dating by Vannay et al. (2004) suggests Munsiari Thrust developed during 4–7 Ma from the Sutlej valley, Himachal Pradesh, India. Catlos et al. (2002) interpreted that the Munsiari Thrust emplaced ~ 5.9 ± 0.2 Ma based on Th–Pb monazite dating (also see ~ 5-4 Ma age recently deduced by

Table 3
Paleostress analyses results from different software. For SG2PS, T-Tecto and WinTensor σ_1, σ_2 and σ_3 represents principal stress axes.

Sense of Movement	SG2PS (trend/plungein degree)			Figure no.	T-Tecto (trend/plungein degree)			Figure no.	WinTensor (trend/plungein degree)			Figure no.
	σ_1	σ_2	σ_3		σ_1	σ_2	σ_3		σ_1	σ_2	σ_3	
Top-to-NW down & top-to-SE down	203/90	43/0	313/00	$16a_1$	180/88	32/2	123/2	$16b_1$	315/88	222/0	132/2	$16c_1$
Top-to-NW up & top-to-SE up	315/0	45/0	217/90	$16a_2$	309/6	40/3	149/81	$16b_2$	317/8	225/11	83/77	$16c_2$

Montemagni et al., 2020). However, an older age of ~19.8 ± 2.6 Ma for the Munsiari Thrust was also noted by Metcalfe (1993), Ar/Ar dating on hornblende.

Brittle deformation study reveals that the NE-SW compression (correlated with D_1 by Hintersberger et al., 2011) predates the NW-SE arc-parallel compression. Ductile to brittle deformation transition within the Himalaya as well as the NE-SW compression happened possibly around 15–17.5 Ma (Hintersberger et al., 2011). Hintersberger et al. (2011) reported NE-SW extension (D_3) within LHS ~ 4–7 Ma based on $^{40}Ar/^{39}Ar$ datingof white mica from the LHS (Sutlej valley).This can be correlated with the NW-SE compression.

5.3. Seismicity & subsurface information

The LHS is one of the most seismically active regions in the mountain belt (e.g., Molnar et al., 1973, review in Rajendran et al., 2017, Fig. 5 for compiled plots in the study area). The International Seismological Center (ISC) data reveals 44 moderate to large earthquake events ($5 \leq M_L \leq 6.3$) in last 60 years (in between 1958 and 2017) in the Kumaun-Garhwal Himalaya (Pasari and Arora, 2017). Between April 2005 to June 2008, Kanna and Gupta (2020) identified 27 earthquakes of $M_L \leq 3.5$ in the Garhwal Himalaya. Within the ILHS, most of the seismic activities are recorded in between the Berinag Thrust and the Munsiari Thrust (Kanaujia et al., 2016). Besides, scattered seismicity was also observed in between the Berinag Thrust and the Tons Thrust, however, mostly restricted in the vicinity of the latter. Most of the

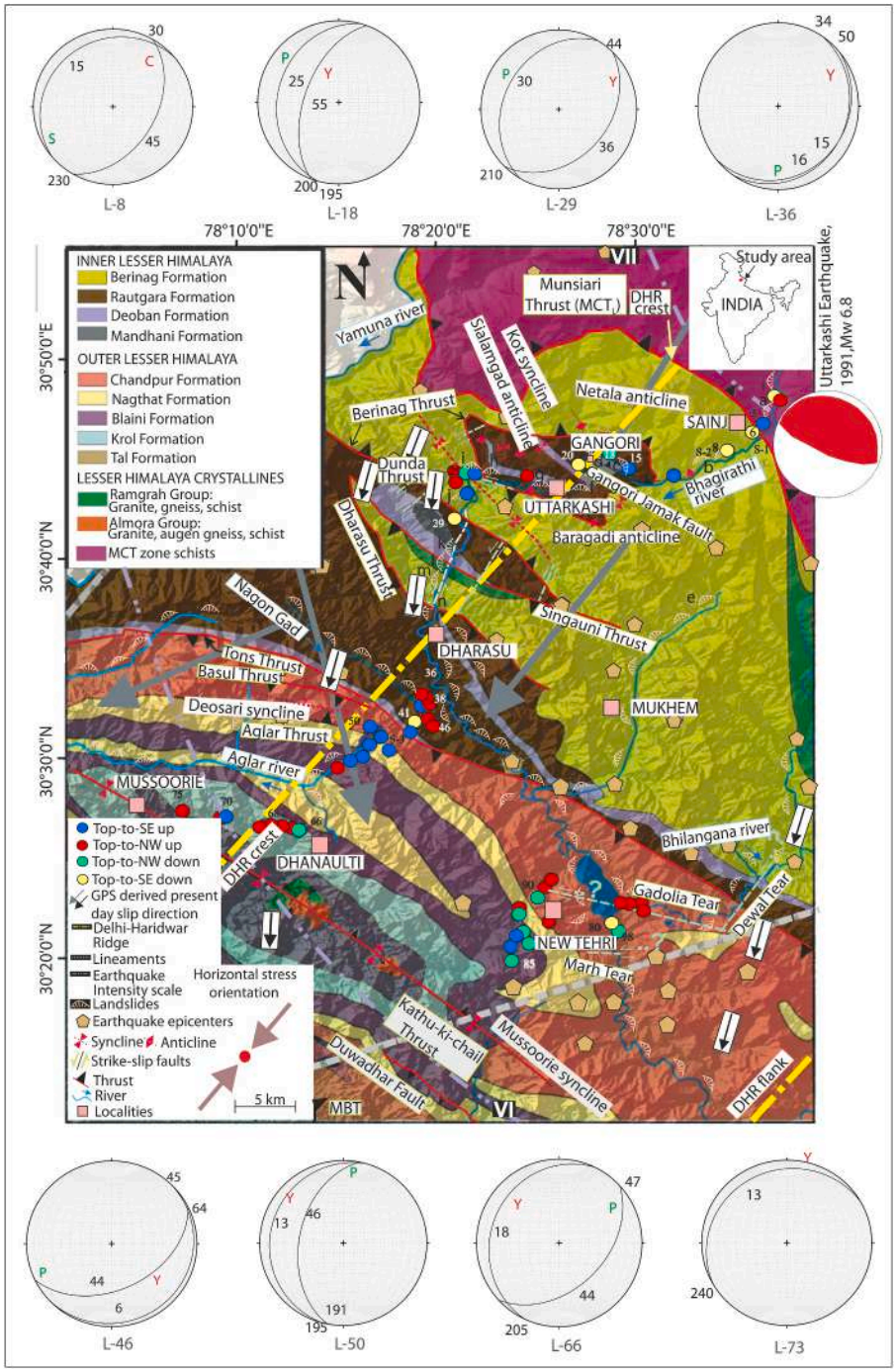

Fig. 5. Field locations plotted on a geological map of the Garhwal Lesser Himalaya Sequence Taken from the compilation made by Bose and Mukherjee (2019a). Stress orientation acquired from Zoback et al. (2009). Lineament orientations are derived from Arora et al. (2012) and Godin and Harris (2014). GPS measurement based on displacement rate (Kundu et al., 2014 and references; Gautam et al., 2017 and references). Structural information of major faults taken from Jain (1975); Jain and Varadaraj (1978); Kumar and Dhaundiyal (1980); Bhatt and Saklani (1990); Sharma and Bhatt (1990); Bhatt and Saklani (1994); Bagri (2006b); Godin et al. (2019) and Bose and Mukherjee (2019a). Topographic data taken from USGS website. Focal mechanism data taken from Jade et al. (2014). Earthquake epicenter data compiled from Paul (2010); Arora et al. (2012); Bose and Mukherjee (2019a), and Kanaujia et al. (2019)- with magnitudes ranging $1 < M < 5$. Earthquake intensity scale data taken from Rajendran et al. (2018). Joshi et al. (1999) deciphered that the aftershock distribution of the Munsiari Thrust caused the 1991 Uttarkashi earthquake, and that it not strongly follow any particular fault trend. Landslide data compiled from Mithal (1988); Bagri (2006a); Bagri (2006b); Sarkar et al. (2011); Gupta et al. (2016); Kumar and Anbalagan (2016); Bhambri et al. (2017) and Nair and Singh (2020). Landslide details: a. Lata ghatori slide b. Aungi slide c. Natala slide d. Ganesh pur slide e. Pinswar slide f. Varunavatslide g. Badhethi Chungi Slide h. Bandarkot Slide i. Raturi Sera Slide j. Singoti Slide k: unnamed l: unnamed m: unnamed. Dharasu Bend 1 and 2. n. Surabhi resort landslide. Landslide images in the study area are provided in the repository. S: sample location. Numbers represents field locations. Alphabet represents landslides. Four types of arc-parallel shears identified from the fieldwork: (i) blue: top-to-SE up, (ii) red: top-to-NW up; (iii) green: top-to-NW down, and (iv) top-to-SE down. Numbers inside stereoplots represent strike and dip.

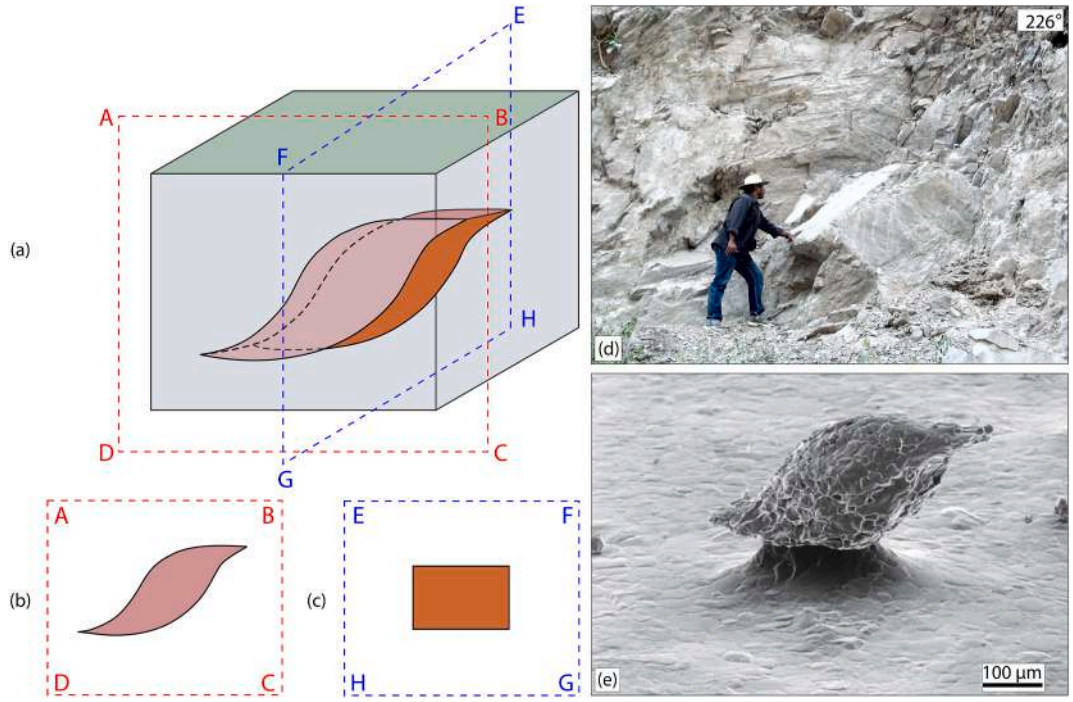

Fig. 6. (a) Schematic diagram: 3D sigmoid inside a solid box. Onto the two vertical planes ABCD and EFGH appearance of the sigmoid are presented in (b) and (c), respectively. (d) Natural example of a 3D sigmoid showing top-to-SW (up) sense of shear from the Rautgara Quartzites, as observed in the field. Height of the person: ~172 cm. (e) Micro-scale 3D sigmoid of quartz fish (after Fig. 5.35 in Passchier and Trouw, 2005). Fig. 6d snapped from near-vertical road-sections from the study area.

earthquake focal points are 30–50 km deep below the LHS (Thakur, 1992). The 20-Oct-1991 6.8 Mw earthquake in the Uttarkashi area and the 28-March-1999 6.5 Mw earthquake at the Chamoli area are the two major seismic events in the Garhwal Lesser Himalaya (Khattri et al., 1994; Kayal et al., 2002). Kumar and Mahajan (1994) reported maximum damage in between Bhatwari and Gangori area due to Uttarkashi Earthquake. Low value of fractal dimension of earthquakes in the Garhwal Himalaya indicates that the main faults (MFT, MBT, MCT)

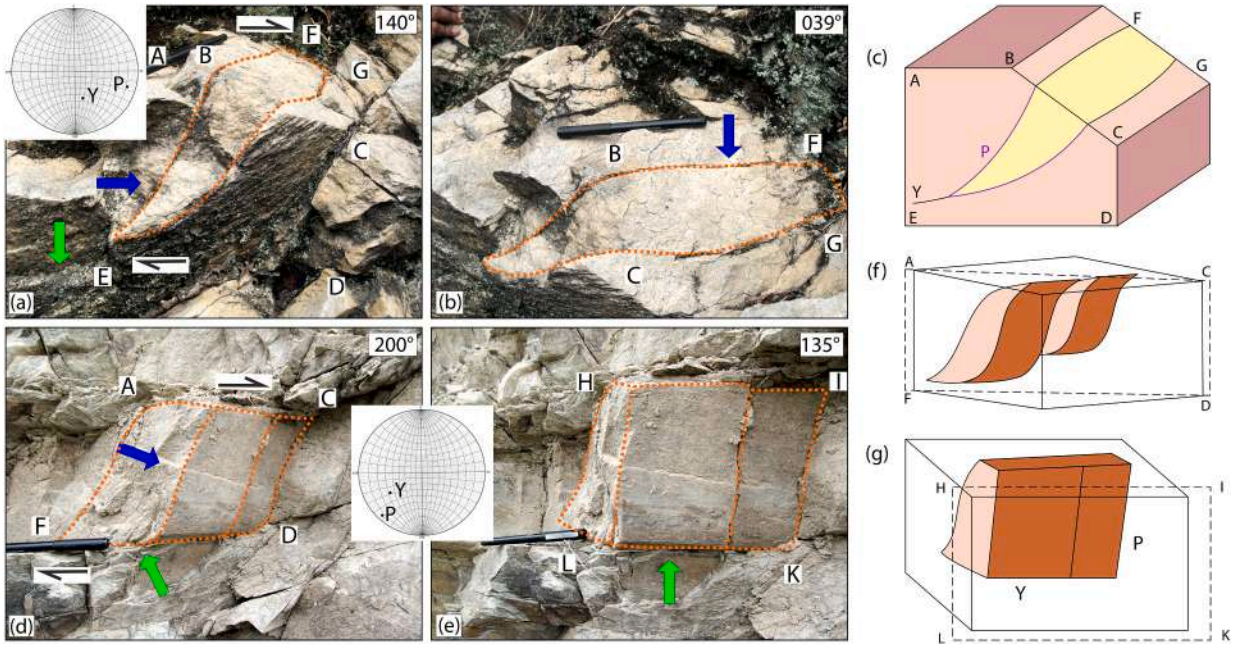

Fig. 7. 3D sigmoid illustrating brittle shear sense (a) Partly broken sigmoid (orange dashed lines) from the Berinag Quartzites, exhibits top-to-SE (up) shear in sectional view where a single Y-plane (dip/dip direction: 36°/340°, marked by green full arrow), is fairly developed. (b) P- planes (dip/dip direction: 76°/280°, marked by blue arrow) are partially preserved. (c) Schematic diagrams of the sections ABCDE and BCGF as in (a) and (b), respectively. The P- planes appear as parallel planes in the section BCGF, similar to Fig. 6c. (d) Top-to-SW (up) sense of shear (sigmoid marked by orange dashed line) in the Rautgara Formation (Green arrow: Y-plane, dip/dip direction: 45°/53°; blue arrow: P-plane, dip/dip direction: 81°/40°). (e) Shear sense absent along 135°–315° section for the same sigmoid (marked by orange dashed lines). (f, g) Schematic diagrams explaining the absence of shear fabric, when viewed in different sections i.e., ACDF vs. HIKL. Fig. 7a,b,d,e are snapped from near-vertical road-sections.

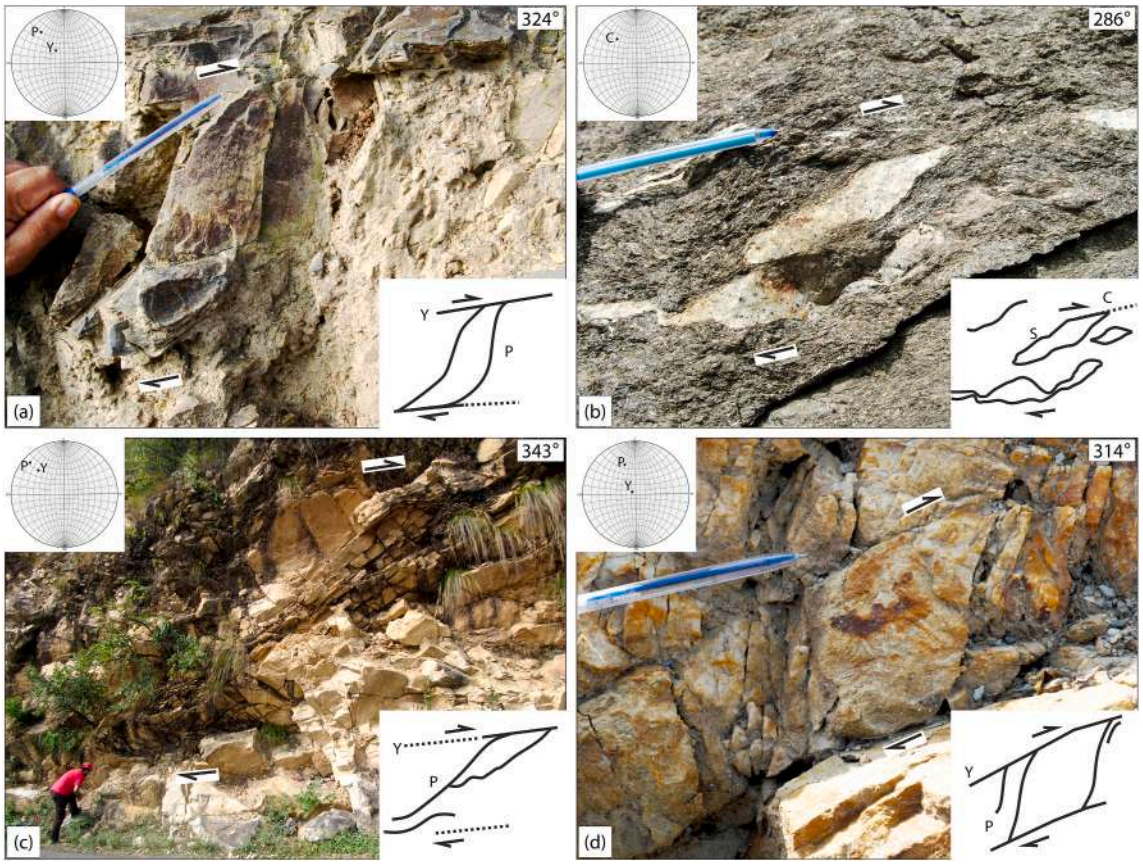

Fig. 8. Field evidences of top-to-NW/WNW(up) shear documented along the Dehradun-Uttarkashi transect in the NW Lesser Himalaya Sequence. (a) Sigmoid P-planes (dip/dip direction: 60°/150°) bounded by Y-planes (dip/dip direction: 17°/150°) within Rautgara Slates. (b) Quartz fish in MCT Zone Schist showing ductile shear (C-plane orientation: dip/dip direction: 45°/130°). (c) Brittle shear zone within the Berinag Quartzite with well-developed Y- (dip/dip direction: 45°/130°) and P-planes (dip/dip direction: 70°/130°). (d) Curved P-planes within the Nagthat Quartzite. Y-planes (dip/dip direction: 6°/135°) are sharp. P-plane- dip/dip direction: 44°/154°. Insets displays the respective stereoplots and sketches. All the images are snapped from near-vertical road-sections.

are primarily responsible for seismicity (Teotia et al., 1999).

The present day GPS-derived stress direction broadly trends SSW/SW direction. However. a subordinate/anomalous SSE trend has also been reported (Gautam et al., 2017 and references therein). The later is worth mentioning in the context of arc-parallel rock movement (Fig. 5).

The ~ NE-SW trending Delhi-Haridwar Ridge (DHR; Arora et al., 2012, also referred as Delhi-Haridwar-Harsil ridge in Bagri, 2006a,b: yellow dash line in Fig. 5), a northward protrusion of the Aravalli range, lies underneath the LHS from 28° N to 30° N to 76°–79° E (Verma et al., 1995). Small-scale transverse structures within Lesser Himalaya having similarities with Aravalli trend gives the first indication of extension of Aravalli range underneath the Himalaya (Valdiya, 1976 and references therein). The northernmost end of the ridge has remained indeterminate. Godin and Harris (2014) suggest that the ridge continues up to the Karakorum Fault.As per one view, DHR's northern extension is up to Uttarkashi (Bagri, 2006a). However, Kanaujia et al. (2016) proposed that the DHR does not extend beyond the MCT, with an offset at the Tons Thrust. This subsurface ridge has possibly affected the stress field, seismicity, and the exhumation rate in its vicinity, and played a major role in deforming the LHS (e.g., Khattri, 1992; Raval, 1995; Bollinger et al., 2004; Gahalaut and Kundu, 2012; Ravi Kumar et al., 2013; Srivastava and Cobbold, 2014; Godin and Harris, 2014).

5.4. Landslides

Areas with high slope, area affected by seismic events, unconsolidated soil, barren land, high relative relief (150–200 m), joint sets, slopes facing south, near road, near drainage, near reservoir and areas near geological structures/weak planes are susceptible for landslides in the study area (compiled in Fig. 5; e.g., Saha et al., 2002; Bagri, 2006b; Pareek et al., 2013; Kumar and Anbalagan, 2016). The detail is presented in Repository 4.

6. Present work

6.1. Field observations

Structural fieldwork was carried out from ~10 km NE of Uttarkashi up to Mussoorie along the National Highway-34, and State Highway-30 for a total of ~152 km in the LHS. Exposures of schists, phyllites, slates, quartzites, dolomites, conglomerates and limestones occur, covering a part of the MCT schist zone, and all of the ILHS and OLHS.

Y-plane/boundary faults and P-planes/Riedel shears, sigmoid rock bulges and vein geometries are utilized from the sub-vertical road sections to decipher the shear senses. Shear movements perpendicular to fore and back structures are documented in this study to understand the deformation produced.

We encountered two cases of 3D-sigmoidal bulge of sheared rock mass (Figs. 6 and 7). In both the cases, the sigmoid geometry is preserved only on the NW-SE sections (Fig. 6d; 7a,d) and not on the NE-SW sections. In the later rock section, the sigmoids manifest merely as parallel straight lines (Fig. 6c; 7 b,e,g) and thus are unsuitable for shear sense determination. Although the field transect trends ~ NE-SW, local turns along the road sections allow us to study NW-SE sections selectively. To pick up arc-parallel deformation we documented four categories of brittle shear senses on the NW-SE sections: (a) top-to-NW up

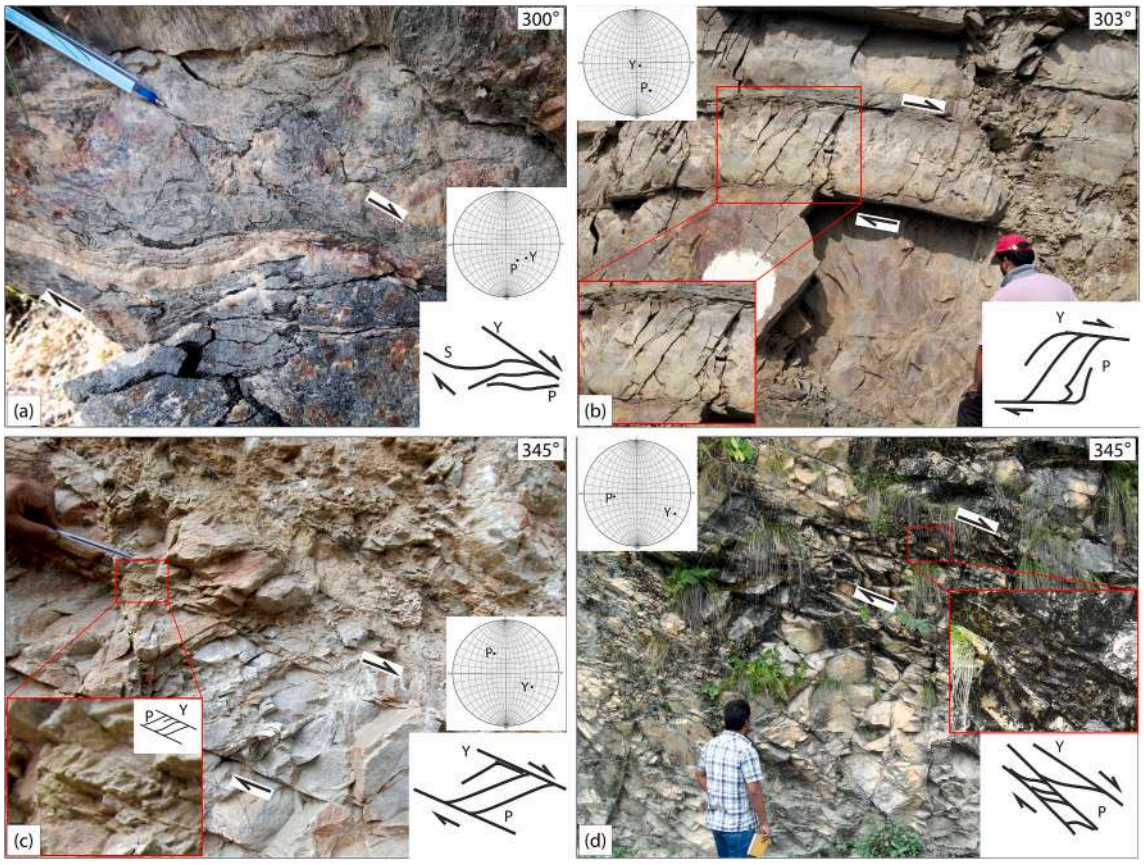

Fig. 9. Field evidences of top-to-NW down shear documented along the Dehradun-Uttarkashi transect in the NW Lesser Himalaya Sequence. (a) Plastically deformed sigmoid quartz-mica-rich layer. The biotite-rich layers (cleavage domains) deformed in a brittle manner (see inset), MCT Zone Schist. Y-plane orientation: dip/dip direction: 40°/300°; P- plane orientation: dip/dip direction: 35°/310°. (b) Brittle sub-horizontal shear zone with distinct Y- and P-planes in the Nagthat Quartzite. Y-plane: dip/dip direction: 5°/224°; P-plane: dip/dip direction: 45°/335°). (c) Sigmoid P-planes (dip/dip direction: 27°/162°) bound by well-developed Y-planes (dip/dip direction: 37°/285°) within the Berinag Quartzite. (d) Y-planes are near parallel to the bedding within the Berinag Quartzite, and the P-planes are curved (Y-plane orientation: dip/dip direction: 50°/290°; P-plane orientation: dip/dip direction: 25°/79°). Insets display the respective stereoplots and sketches. All the images are snapped from near-vertical road-sections.

(Fig. 8), (b) top-to-NW down (Fig. 9), (c) top-to-SE up (Fig. 10), and (d) top-to-SE down (Fig. 11). However, lack of cross-cut relations amongst these shears prevents from drawing their relative temporal relations.

6.2. Microstructural study

Three oriented rock samples – two biotite schists (samples S1 and S2) and a single quartz-mica phyllite (sample S3) – are collected from the ILHS and the OLHS, respectively. The purpose is to examine and confirm the presence of arc-parallel shear at micro-scale, which otherwise looks ubiquitous in the meso-scale. In all other field locations we confirmed the arc-parallel shear based on the well-known shear sense indicators, therefore, we did not go for thin-section studies from rocks from those locations. Samples S-1 and S-2 (Fig. 5) come from the Berinag Formation and are collected from the footwall of the Munsiari Thrust. The outcrops for S-1 and S-2 exhibit top-to-NW up (Fig. 12a). and top-to-SE down (Fig. 12b) shear senses, respectively. The sample S-3 (N30°32.841'; E 78°19.437', Fig. 5) comes from the Chandpur Formation, and shows a top-to-NW up shear at meso-scale (Fig. 12c and d).

Thin-sections parallel to the dip directions [section trends for S-1 (110°–290°), S-2 (165°–345°) and S-3 (101°–281°) and perpendicular to the primary shear planes are prepared. In absence of clear-cut lineations in the field (e.g., Piazolo and Passchier 2002), planes which are near perpendicular with the line of intersection between P- or S- plane with Y- or C- plane are chosen. Attitude of the main foliations (primary shear planes) are ploted in Fig. 5. The purpose is to confirm the shear sense in micro-scale where we had doubt in shear sense observed in the field. In the subsequent paleostress analyses, we incorporated field data, and no inputs were taken from these thin-sections. Significant grain size reduction, alterations of existing minerals (mainly feldspar), recrystallization, shear fabrics etc. indicate that the rocks are significantly deformed in ductile and brittle regimes. S-1 and S-2 show ductile features viz., as S–C fabrics (Fig. 13c), quartz ribbons (Fig. 14d) and partial recrystallization of feldspar grains (Fig. 13d). S-3 consists of typical brittle deformation features e.g., extensional joints (Figs. 13a and 14b) and curved fracture planes and grain-size reduction (Figs. 13a and 14b). Curved extensional brittle plane developed within quartz-sericite mylonite (Fig. 13a), and partly altered sigmoid feldspar porphyroclast within biotite-rich matrix (Fig. 13b), biotite fish within mylonitized matrix (Fig. 14c) and asymmetric ribbon of quartz within biotite matrix (Fig. 14d) show a top-to-SE shear. Top-to-NW shear is recorded as curved quartz vein within the quartz-sericite mylonitic matrix (Fig. 14b) and partly recrystallized sigma-shaped feldspar within the mylonitic matrix (Fig. 13d) near the MCT. Sigma-shaped aggregates of fragmented feldspar pophyroclasts bound by steeply (Fig. 13c) and gently (Fig. 15b) dipping C-planes near the MCT zone record a top-to-NW down shear. Top-to-SE up shear is represented by sigmoid biotite fish (Fig. 14a) from the mylonitic schist of the Berinag Formtion. Extensional shear (top--to-SE down) (Fig. 15a) is also observed from the quartz-feldspar-biotite mylonite.

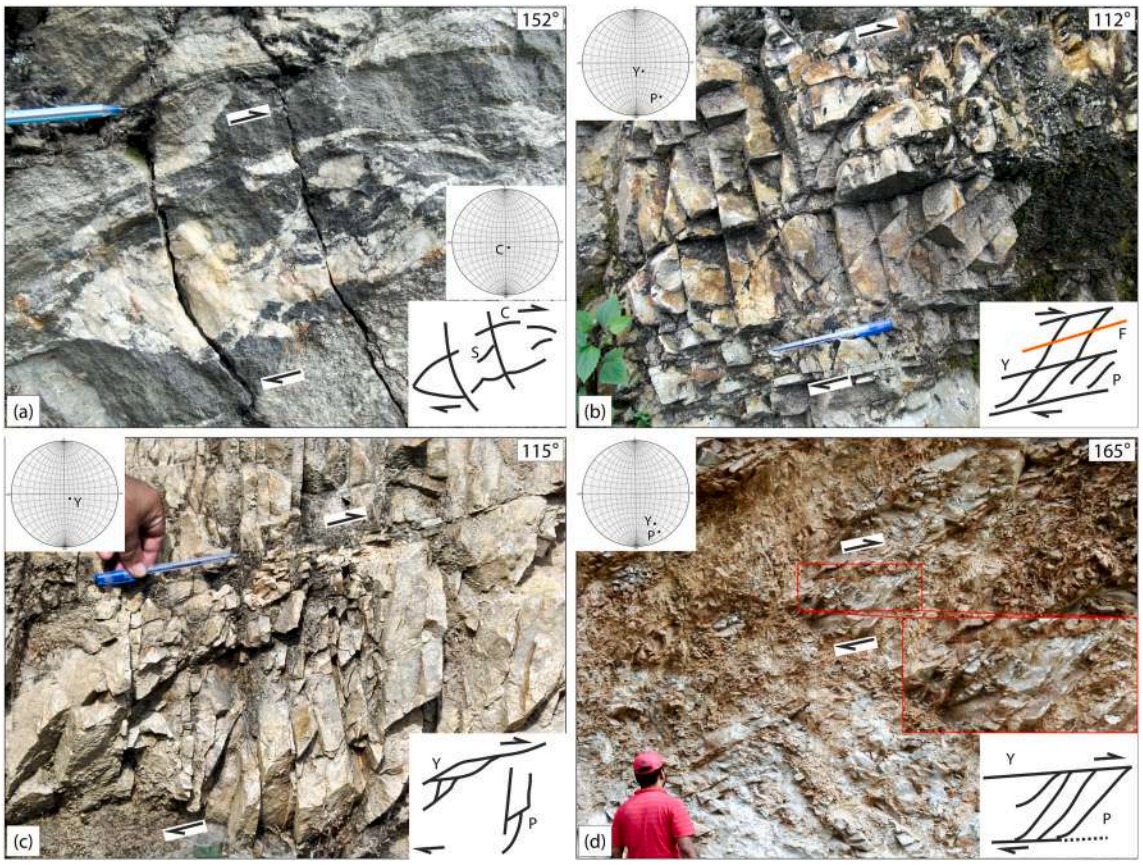

Fig. 10. Field photographs of top-to-SE (up) shear documented along the Dehradun-Uttarkashi transect in the NW LHS. (a) Quartz-mica rich layer (microlithons) ductile shear in cm-scale (C plane orientation: dip/dip direction: 10°/345°) which was later underwent brittle deformation-devoid of any shear sense, MCT zone schist. (b) Two sets of brittle shears developed (Y- plane orientation: dip/dip direction: 19°/321°; P- plane orientation: dip/dip direction: 53°/323°) within the Rautgara Quartzite revealing top-to-SE (up) shear sense. A fracture developed near parallel to the Y-plane (mark by orange color: F). (c) Brittle shear zone within the Nagthat Quartzite. Y- planes (dip/dip direction: 13°/346°) bound the poorly developed P-planes. (d) Brittle top-to-SE (up) shear exhibited within the Berinag Quartzite. Y-planes (Y- plane orientation: dip/dip direction: 37°/338°; P- plane orientation: dip/dip direction: 60°/336°) are sub-horizontal, developed at 29° angle with the bedding and P-planes are gently curved. S. Mukherjee as marker (height, elbow to head ~ 80 cm). Insets display the respective stereoplots and sketches. All the images are snapped from vertical road-sections.

6.3. Paleostress analysis

Repository 5 presents the principals involved in this study.

6.3.1. Steps

84 fault kinematic data viz. brittle Y-, P-planes/riedel shears; S-, C-planes; sigmoids; vein geometries (assumed to represent the outcomes of the youngest deformation in this region) have been documented from more than 98 locations in the field (locations in Fig. 5). Plane Y- and plane C- attitudes are separately processed using three paleostress analysis software: (i) SG2PS (V.2), (ii) T-TECTO (Studio X5), and (iii) Win-TENSOR (5.8.8; detailed in Repository 5). Paleostress analysis has been recommended to be run by different means in order to confirm the results (Simón, 2019). Field data exhibits an abundance of gently to moderately dipping fault/shear planes and few steeply dipping ones. Due to lack of striation data, movement along the fault/shear plane was assumed to be dip-slip in nature. This is a standard assumption adopted by field geologists. Y-Plane/C-plane are considered to be the fault planes, along with the geographic direction of movement i.e. NW or SE For this study. The analyses are carried out to identify primarily the paleostress principal axes orientations.

The data to be input by the user for each of the software are presented in the Appendix-A.

Slip senses collected from the field are classified into four categories. (i) Top-to-NW up, (ii) top-to-SE up, (iii) top-to-NW down, and (iv) top-to-SE down. Subsequently, the entire dataset is used as input and the software clubbed them into two groups based on their two sets of slip-senses supposedly developed under the same stress regime.

6.3.2. Results (Table 3, Fig. 16)

Comparison on the aforementioned three paleostress software reveals a close match in between WinTensor and SG2PS results, however, T-Tecto displays not a very significant deviation (~5–11°) in the orientation of principal stress axes with others. This happens because the software has different statistical ways of analyzing the data.

Principal stress axes in SG2PS are oriented following Andersonian stress regime, i.e., orthogonal to each other with two stress axes lying horizontal. Whereas, for T-Tecto and WinTensor, the principal axes orientations remain near ~ orthogonal and creating a very low angle with the horizontal orientation. With all the 84 data input, SG2PS identifies two deformation events, marked by two different orientations of principal stress axes (Table 3), however, represents the result in a single stereo-plot superposing the results one on the other. This often forces the user to identify, separate and define the data group beforehand. From Win-Tensor, additionally, stress ratio ($R = \sigma2\text{-}\sigma3/\sigma1\text{-}\sigma3$: Delvaux and Sperner, 2003) can be derived and then the stress index (R') can be obtained. For example, for extensional stress tensor $R' = R$, strike-slip stress tensor $R' = (2\text{-}R)$ and under compressional stress tensor type $R' = (2 + R)$. Based on the stress index, stress regimes can be of various types. For example, for top-to-NW up and top-to-SE up shears in

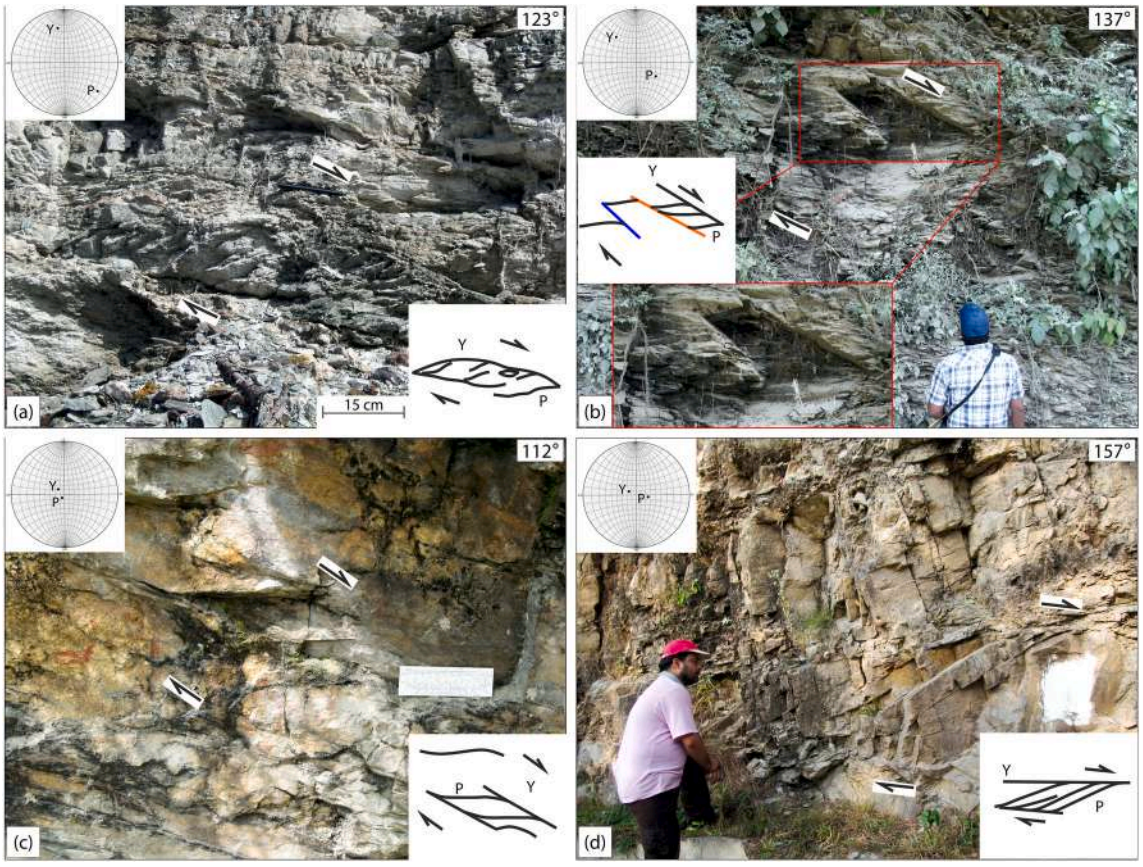

Fig. 11. Field evidences of top-to-SE down shear documented along the Dehradun-Uttarkashi transect in the NW Lesser Himalaya Sequence. (a) Curved Y-planes (dip/dip direction: 17°/150°) bound the P-planes (dip/dip direction: 25°/285°) in the Rautgara Slates. (b) Brittle shear zone within the Rautgara Quartzite consisting sharp Y-planes (dip/dip direction: 36°/134°) and fairly developed P-plane (dip/dip direction: 30°/300°), different set of Y-planes (marked by blue and orange lines, respectively) are non-parallel. (c) Sigmoid P-planes (dip/dip direction: 8°/50°) bounded by poorly developed Y- shear planes (dip/dip direction: 16°/135°) within the Berinag Quartzite. (d) Curved Y- (dip/dip direction: 7°/104°) and P-planes (dip/dip direction: 24°/264°) within the Nagthat Quartzite. Well defined Y-planes parallel the bedding plane. Steeply dipping fractures are locally sub-parallel to P- plane. Insets display the respective stereoplots and sketches. All the images are snapped from near-vertical road-sections.

our study area, $R' = 2.73$ indicates pure compressive regime. For top-to-NW down and top-to-SE down shears, $R' = 0.21$ denotes radial extensive stress regime. However, Win-Tensor software has a limited control over dataset and often seen to be using a selected amount of data thus neglecting the remaining data, which may have an influence in the paleostress results. For example, the software considered only 72 fault data as good data amongst 84. By analyzing the paleostress data using different methods, we checked the authenticity of the results.

Rarely, T-Tecto neglects any data from dataset. It segregates individual deformation phases and generates two different plots smoothly.

7. Discussions

The new data set consists of attitudes of meter to cm-scale shear planes (foliation plane in case of ductile shear and fault plane/Y-plane for brittle shear) documented along the Bhagirathi section from ~10 km NE of Uttarkashi up to Mussoorie.

Arc-parallel extension and compression are omnipresent throughout the area. Few areas are affected with denser data under the influence of major regional structures. Such locations are the hangingwall and on the footwall blocks of the Tons Thrust, Berinag Thrust and around the Mussoorie synclinal axis. Based on field observations from HHC, arc-parallel extension within NW Himalaya was earlier predicted to be extended in lower elevation such as the LHS (Hintersberger et al., 2011). The prediction is re-iterated by the field evidences cited in the present study.

Pre-Himalayan extensional and compressional events, though reported from various places from the orogen, are scarce (Repository 1). NE-plunging isoclinal folds have been reported from the Kumaon Himalaya (Patel et al., 2011) parallels the orogenic trend. Abundant and prominent arc-parallel deformation features within the Garhwal LHS indicate the recorded deformations are much recent events. Overall acceptance of pre-Tertiary deformations within Himalaya is still unpopular and in various cases recorded pre-Himalayan deformations were later linked with Himalayan deformation as the understanding of the orogeny upgraded (Bhargava et al., 2011). However, reactivation of pre-existing weak planes belonging to Indian plate is capable of producing deformation within the cover rock (Godin et al., 2019).

The Dehradun lineament (Fig. 2) underlying the study area trends NW-SE can be linked with arc-parallel extensional shear fabrics. From Fig. 2, a rough correlation can be drawn in which extension around Leo-Pargil dome, Zada basin, NW Tethyan and Higher Himalayan extension are correlated with the Dehradun lineament. The Gurla-Mandhata-Humla fault system can be linked with lineament situated in between the Dehradun and the Lucknow lineament. Extension in the Marsyandi valley and in the Malashan Dome can be associated with the Pokhara lineament. Occurrence of the Kangmar Dome can be tied with the 88°E lineament. The Kolkata lineament possibly has a connection with the NE Higher and the LHS extension.

Paleostress analyses using three software in this work identified that the arc-parallel compressional shear direction is 131°-311° and that for the arc-parallel extension is 133.5-313.5°.

Fig. 12. Structures along the Mussoorie-Uttarkashi transact in the NW Lesser Himalaya Sequence. Sample locations plotted in Fig. 2. (a) Sample S-1. Sigmoid feldspar porphyroclast[top-to NW (up) slip] within the Berinag Formation. The length of the pen visible as marker is ~5 cm. Attitude of C- plane: 45°/130° (dip/dip direction; measured outside photograph). (b) Sample S-2. Distinct S- and P- brittle planes show top-to-SE down slip within the Berinag Formation. S. Mukherjee as scale (waist to head height ~ 80 cm). Attitude of the C- and S- planes: 20°/155° (yellow arrow) and 52°/170° (red arrow), respectively. (c) Sample S-3. Brittle shear zone in the Chandpur Formation with Y- and P-planes showing top-to-NW (up) slip. S. Mukherjee as scale (height ~ 174 cm). (d) Zoomed portion of (c) with sigmoid P-planes (68°/138°; red arrow) bound by distinct Y-planes (30°/105°; yellow arrow) within the Chandpur Formation.

7.1. Possible mechanisms for arc-parallel deformation (extension and compression) in NW Indian LHS

The arc-parallel extension in the NW Indian LHS could be explained by: (i)"radial thrusting and expansion model" combining arc-geometry and major thrust fronts (e.g. Seeber and Armbuster, 1984; Murphy et al., 2009), (ii) "removal of mantle" (e.g. England and Houseman, 1989), (iii) accumulation of mass and energy under collision and dissipation of the stored energy (Hodges et al., 2001), or (iv) basement influence on cover (e.g. Godin et al., 2019; Lacombe and Bellahsen, 2016). The "oblique convergence model" (McCaffrey and Nablek, 1998; McCaffrey, 1996) can explain both arc-parallel compression and extension provided the local stress magnitude exceeds than the regional one (Boutelier and Oncken, 2010). This local stress can either create extension or compression parallel to the arc. Presence of both the arc-perpendicular (NE-SW) and arc-parallel (NW-SE) brittle/ductile shear fabrics – documented in this study from the NW Indian LHS makes the model consistent with either arc-parallel compression or arc-parallel extension. Consequently, alternate mechanisms could be required to address the coexistence. "Gravitational collapse", which discusses escape tectonics can explain arc-parallel shear, however, those brittle structures are more likely to trend E-W and are unlike observations of this work (NW-SE shear) from the field and also under an optical microscope.

Although models such as "orogen bending" and "rigid plate indentor" justify the occurrences of arc-parallel extensional structures within the LHS (and the HHC), they are incompatible to develop arc-parallel shears at the eastern and the western portions of the Himalaya. The NW Indian Lesser Himalaya Sequence is devoid of extruded domes, thus we can dismiss "dome extrusion"-induced extension in the region.

Table 4 presents the models and their chances of occurring arc-parallel extension.

7.2. Most suitable model(s) for arc-parallel extension in NW Indian LHS

The model "radial thrusting and extension" incorporate the southward migration of the thrust fronts along with their arcuate geometries. It addresses the development of NE-SW striking extensional features in the NW Indian LHS due to arc-parallel stretching, to preserve the arcuate geometry of the orogen. Within NW Higher Himalayan Crystalline both ductile and brittle shear fabrics are correlated with the aforementioned model (Hintersberger et al., 2011).

Lithosphere underneath the collisional margin experiences "convectional thinning" and thus develops rifts. Through such rifts are found in Tibet, these are rare within the Himalaya. Several authors (e.g., England and Houseman, 1989) attempted to correlate Himalayan arc--parallel extension with thick-skinned tectonics. Validity of such a model would require a deeper insight and thus remains as a possibility to explain arc-parallel shear within NW Indian Himalaya.

Taloor et al. (2021) identified five levels of river terraces based on geomorphic studies from the Garhwal LHS. Pandey et al. (2005) recorded five stages of uplift. These point out that the "mass accumulation and stored energy dissipation" has occurred in the LHS. Dharasu and Varunavat (Fig. 5 for location; e.g., Sarkar et al., 2011; Joshi et al., 2003)

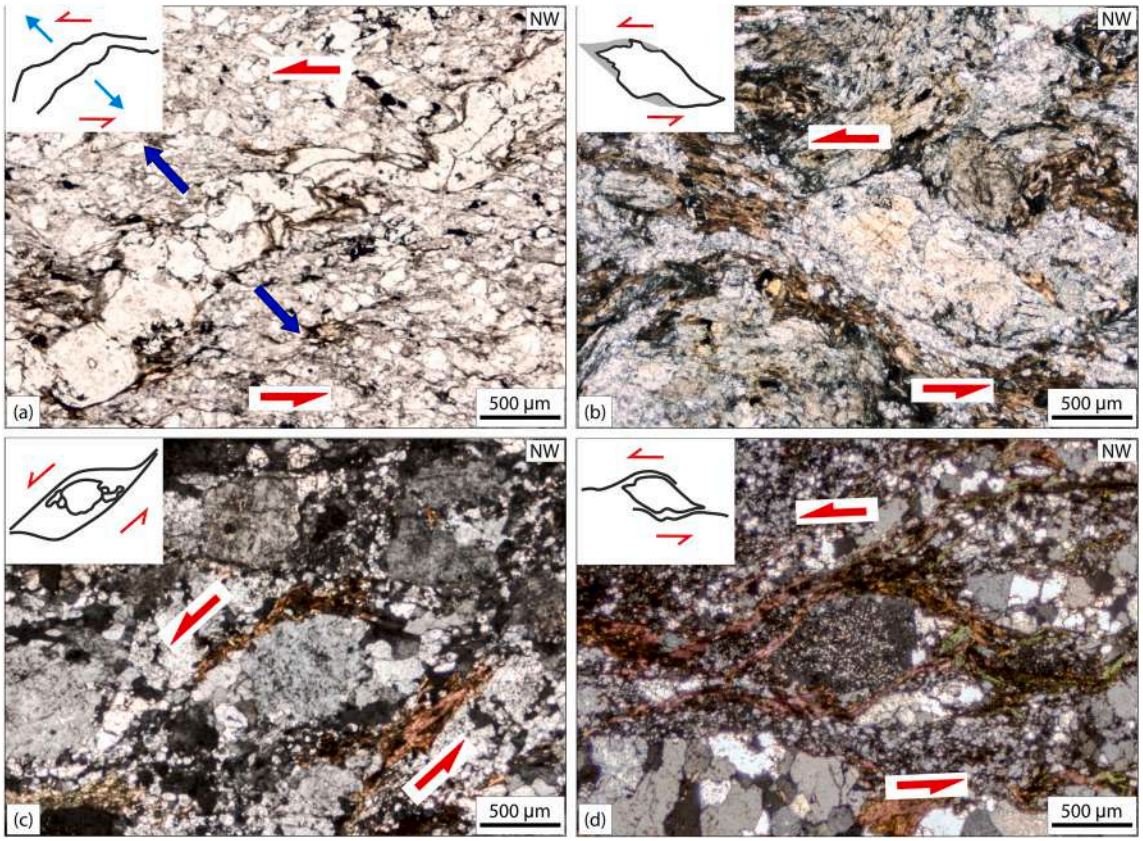

Fig. 13. Photomicrographs exhibiting brittle and ductile shear. (a) Mylonitization in the quartzite, feldspar grains transforming to sericites and significant grain-size reduction. The extensional quartz vein cross-cuts the original rock and indicates top-to-SE shear (under plane-polarized light, Chandpur Phyllite, hangingwall of the Tons Thrust). Sample belongs from OLHS. (b) Sigmoid shaped, partly altered feldspar porphyroclast within a biotite-rich matrix. Top-to-SE slip (cross-polarized light, Biotite-schist of the Berinag Formation, footwall of Munsiari Thrust/MCT_L, NW Inner Lesser Himalaya Sequence). (c) Fractured feldspar porphyroclasts with fragmented tails partially bound by plastically deformed, elongated biotites, defining local foliation plane. Top-to-NW down slip (cross-polarized light, Berinag Formation, Inner Lesser Himalaya Sequence, footwall of Munsiari Thrust/MCT_L). (d) Sigmoid feldspar porphyroclast with poorly developed C-plane wrapped by elongate biotite grains within mylonitic matrix. Top-to-NW-horizontal slip (cross-polarized light, Berinag Formation, Inner LHS, footwall of the Munsiari Thrust/MCT_L).

are localities around which severe landslides have been reported. Besides, frequent landslides along the existing river pathways in the LHS have been common (locations in Fig. 5). Theoretically, landslides are in direct link with geological structures, earthquake epicenters, high relative relief, joint sets, slopes facing towards the regional rock movement (S direction), apart from human activities such as road and reservoir construction. Squandering of accumulated energy in form of landslides, erosional activites within Garhwal Himalaya under tectonic influence is well evident. Arc-parallel extension towards NW-SE trend is thus can be correlated with such process.

The fourth and the final possibility ("basement influence on cover") for the arc-parallel extension involves thick-skinned tectonics, in which the subsurface pre-existing surface plays a crucial role in deforming the surface structure. The Delhi-Haridwar ridge (Godin and Harris (2014)) situated below the NW LHS plausibly influenced the surface structure with its additional elevation from the surroundings (Fig. 17a). The DHR has been stated to be the cause of mass movement in Varunavat and also a reason for the Uttarkashi earthquake (Bagri, 2006a). Over-riding mass, experiences an additional stretching (NE-SW trending) and can develop NW-SE extensional structures/shear fabrics (Fig. 17b).

Several ridge and lineaments (Fig. 2) oriented in NE-SW direction within the Indian plate are capable of generating seismic events, modifying river drainage pattern and the Himalayan surface morphology (Godin et a., 2019). As per Godin et al. (2019), based on analogue centrifuge models, the lineaments/basement faults of the Indian plate are capable of producing arc-parallel extension at surface level. Our field-evidence, NE-SW trending extensional shear fabrics above the DHR, justifies this model. It is further premised by us that such kind of shear fabrics exist in the Himalayan rocks overlying these sub-surface lineaments/basement faults (Fig. 2; e.g., Simla, Dehradun, Lucknow, Pokhara, Kathmandu, 88°E, Kolkata linemants; Delhi-Haridwar ridge, Faizabad ridge and Munger-Saharsa ridge). This observation provokes a new opening for future Himalayan research.

The first three hypotheses are regionally significant, especially at higher elevations of the Himalaya-Tibet region. On the other hand, the fourth hypothesis i.e., presence of the DHR would locally influence the Siwalik and the LHS only. The four possibilities are not mutually exclusive and might act in different degrees to produce the arc-parallel extension. Sub-surface presence of the DHR and its direct correlation to the arc-parallel extension is debated, however, we suspect that the high elevation did influence the surface structures in the region.

7.3. Best model for arc-parallel compression in the NW Indian Lesser Himalaya sequence

As per Section 5.2, the "oblique convergence" model – although a popular one, can either justify arc-parallel extension or compression, but not both. This is a major limitation to the applicability of this model in our study area where both the regional (NE-SW deformation: fore-structures) and the local stress-induced structures occurred. Besides, their explanation is conditional i.e. the local stress component should dominate over the regional one.

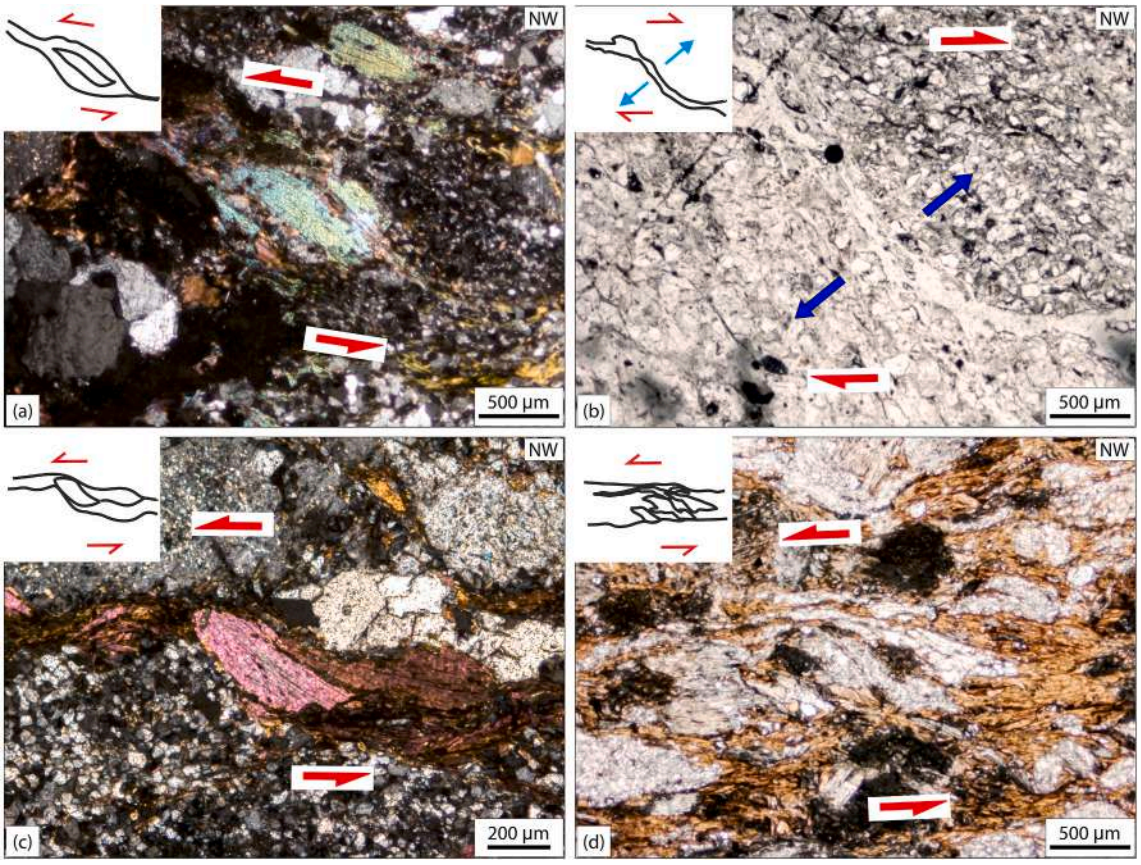

Fig. 14. (a) Mylonitized schist with the biotite fish showing top-to-SE (up) shear. Grain boundary migration along the cleavage planes also documented (Cross-polarized light, Berinag Formation, Inner LHS, footwall of the Munsiari Thrust/MCT_L). (b) Crushed randomly oriented quartz and muscovite grains. Top-to-SE shear deduced from sigmoid-extensional fracture, similar to tensional gash (plane polarized light, Chandpur phyllite, hangingwall of the Tons Thrust. Sample belongs from Outer LHS. (c)Top-to-SE sheared biotite fish. Severely mylonitized quartz grains and altered feldspar porphyroclast lie below and above the C-plane, respectively (cross-polarized light, Berinag Formation, Inner Lesser Himalaya Sequence, footwall of the Munsiari Thrust/MCT_L). (d) Fractured and fragmented sigmoidal imbricated ribbon quartz grains indicate a top-to-SE down slip in pelitic schist. The foliation warp around the quartz aggregate (plane polarized light, Berinag Formation, Inner Lesser Himalaya Sequence, footwall of the Munsiari Thrust/MCT_L).

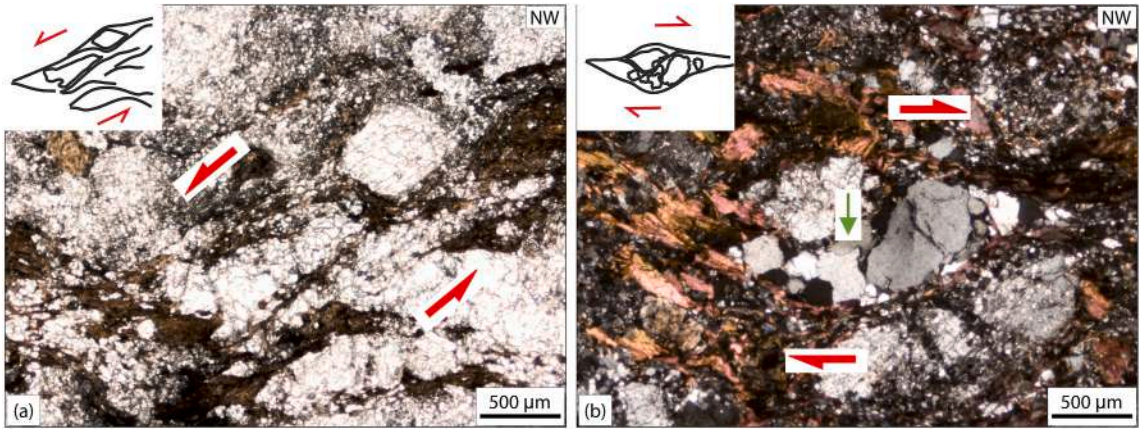

Fig. 15. (a) Feldspar porphyroclasts show a top-to-SE down slip. The plastically deformed biotite grains show elongated behaviour and define the poorly developed foliation plane (plane-polarized light, Berinag Formation, Inner LHS, footwall of the Munsiari Thrust/MCT_L). (b) Grain boundary bulging (green arrow) in quartz. Top-to-NW (right) shear within altered K-feldspar grains (bottom right) bounded by plastically deformed biotite grains. Cross-polarized light, Berinag Formation, Inner LHS, Footwall of the Munsiari Thrust/MCT_L).

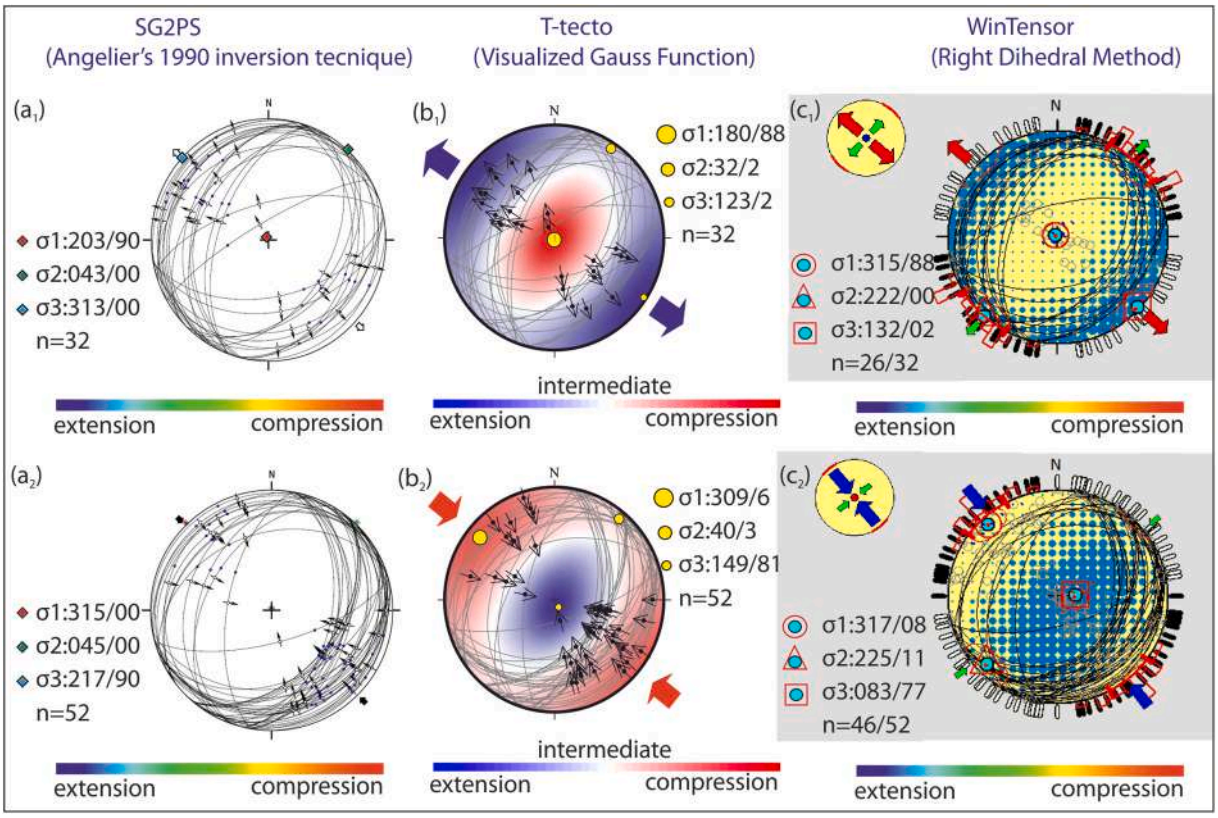

Fig. 16. Paleostress analysis of the observed shear fabrics are enlisted using three different software. Phase 1: (a1, b1, c1) Top-to-NW down and top-to-SE down shear (Extensional shear). Phase-2: (a2, b2, c2) Top-to-SE up and top-to-NW up shear (compressional shear).Analysis of field data using column-1: SG2PS software version 2 (Angelier's inversion technique),column-2: T-Tecto version X5, third column: WinTensor version 5.8.8.Orientation of the principal stress axes are mentioned at the bottom left corner for SG2PS, top right corner for T-Tecto and bottom left corner for Win-Tensor. n = no of data used to run the software. "Results" Section compares outcomes from these columns.

We eliminated the "plate rotation" theory since neither the Indian nor the Eurasian plates are micro-plates or involve any micro-plates in between. This left us with the only model proposed by Seeber and Pêcher (1998): "abrupt termination of the lateral mass-flow". Arc-parallel compression requires an abrupt boundary to prevent the lateral mass--flow. DHR has been well understood already as a barrier to deformation front (review in Manglik et al., 2022). Topographic manifestation of DHR has been reported by geophysicists (Dal Ziilo et al., 2020). South to our study area in sub-surface the elevated DHR can cause an indirect effect to terminate the flowing mass and allow them to pile up, thereby generating arc-parallel compression (Fig. 17c).

Previous workers (Agarwal and Kumar, 1973; Misra and Bhattacharya, 1973; Jain, 1987; Dubey and Jayangondaperumal, 2005) also reported arc-parallel compression from the Garhwal LHS as byproducts of some other studies. Although earlier studies expressed the existence of arc-parallel compressive stress-field, for the first time the present work attempts to genetically correlate arc-parallel compression with basement high (Fig. 17c). It is further predicted such kind of deformation can be observed above the other Himalayan sub-surface ridges.

The Ganga basin south to the Himalaya is typically characterized by two depressions (Sarda deep and Gandhak deep) situated in between three established ridges (Delhi-Haridwar ridge, Faizabad ridge and Munger Saharsa ridge; e.g., Sinha et al., 2005; Negi et al., 1989). Based on geomorphic studies, Goswami (2012) observed a direct link amongst sedimentary thickness, basement highs and reactivated basement faults. Basement structures are capable of bending cover rocks and can bend an orogen itself (Goswami, 2012). Such a structure controlling arc-parallel shear could be possible.

7.4. Relation between arc-parallel shear with landslides, seismicity and regional faults in NW LHS

In this section, brittle and ductile deformation ranging from mm to m-scale and its possible relation and effect are viewed in larger scale taking in consideration of geodynamic framework of the LHS.

Natural landslides in the study area are concentrated along the river section where undercutting of stream plays the most important role. South/south-east/south-west facing planes are more susceptible to landslides upon receiving of heavy rainfall and the direction of rock-movement is overall southward in the Himalaya. SE-dipping planes being a part of arc-parallel deformation thus further provides additional weak zones from which the landslides can initiate, given proper geological and geomorphic settings.

The study area consists of several earthquake epicentres (Fig. 5). GPS derived stress pattern in NW Lesser Himalaya reveals present day SSE-trending stress axis, thus arc-parallel deformations could contribute in generating earthquakes in the LHS. This may further nucleate landslides as observed along the Alakananda valley in the Garhwal Himalaya. After the 28-March-1999 Chamoli earthquake, 56 seismicity-related active landslides occurred in the Garhwal Himalaya (Barnard et al., 2001).

Table 4
Discussion and correlation of arc-parallel deformation in NW LHS and existing models.

Sl. No.	Models	References	Salient point	Figure no.
Arc-parallel extension				
1.	Gravitational Collapse	Davis and Maidens (2003); Takeshita and Yagi (2004); Jolivet et al. (1999); Dalmayrac and Molnar (1981); Molnar et al. (1983); Royden et al., 1997; Molnar and Lyon-Caent (1989); Ratschbacher et al. (1994)	Arc-parallel extensional structures are not expected to develop within NW Lesser Himalaya Sequence, however, development of structures trending east-west is likable.	2i
2.	Radial Thrusting and Expansion	Platt and Vissers (1989); Martínez-Martínez and Azañón (1997) and references therein; Treloar and Coward. (1991); Murphy and Copeland (2005); Murphy et al. (2009); Hintersberger et al. (2011); Seeber and Armbruster (1984); Armijo et al. (1986)	Arc-parallel extensional structures are developed at lower frequency with respect to Higher Himalayan Crystalline	2ii
3.	Orogen bending	Ratschbacher et al. (1994); Kapp and Yin (2001); Robinson et al. (2007); Özsayin and Dirik (2011); Shaanan et al. (2015); Catalán et al. (2014); Bradshaw et al. (1996); Schmid et al. (1998)	Development of arc-parallel extensional structure at NW Himalaya, will not be possible as Central Himalaya is the severely affected region	2 iii
4.	Removal of mantle	England and Houseman (1989); Ansdell et al. (1995); Dilek and Altunkaynak (2007); Hoke et al. (2000); Miller et al. (1999); Mouthereau et al. (2012); Turner et al. (1996)	Development of arc-parallel extensional structure is possible (?)	2iv
5.	Oblique convergence (Type-I)	McCaffrey and Nabelek (1998); Styron et al. (2011); Ellis and Watkinson (1987); Avé Lallemant and Guth(1990)	Development of arc-parallel extensional structure is not possible since the regional stress component > local stress component	2v
6.	Dome extrusion	Ratschbacher et al. (1989); Frisch et al. (2000); Martínez-Díaz and Hernández-Enrile (2004); Viruete(1999); Hetzel et al. (1995); Faure (1995); Thiede et al. (2006); Aoya et al. (2005)	Development of arc-parallel extensional structure is not possible in NW Lesser Himalaya Sequence	2vi
7.	Rigid Central Himalaya	Ratschbacher et al. (1989); Bonini et al. (1999); Robl and Stüwe (2005), Martinod et al. (2000)	Development of arc-parallel extensional structure at NW Himalaya, will not be possible as Central Himalaya is the severely affected region and only the producer of arc-parallel extensional structure	2 vii
8.	Basement influence on cover	Brown et al. (1999); Godin et al. (2019); Lacombe and Bellahsen (2016)	Development of arc-parallel structure is possible under the influence of extension due to the additional elevation underneath, surface migration of pre-existing faults	2 viii
9.	Mass Accumulation and stored energy dissipation	Hodges et al. (2001)	Arc-parallel extensional structures are developed at lower frequency with respect to Higher Himalayan Crystalline	2ix
Arc-parallel compression				
10.	Oblique convergence (Type-II)	McCaffey (1996); Allemendinger et al. (2005); Boutelier and Oncken (2010)	Development of arc-parallel compressional structure is not possible since the regional stress component > local stress component	3i
11.	Plate rotation	Carosi et al. (2004) and references therein; Viti et al. (2004)	Arc-parallel compressional structure is not possible as both Indian and Eurasian plate never underwent significant rotation	3ii
12.	Abrupt termination of lateral mass-flow	Seeber and Pêcher(1998); Biswas et al. (this work)	Development of arc-parallel compressional structure is most credible under the influence of sub-surface high (DHR).	3iii

The Bhagirathi river course within the study area is guided by several zone of weaknesses (e.g., strike-slip faults, thrusts, antiformal and synformal hinges). In addition to such structures, shear planes oriented parallel to arc are well capable of contributing landmass movement along it's weak plane.

At present the study lacks direct link between arc-parallel shears and landslides, earthquake epicenters and regional faults. Nevertheless their close spatial occurrences (Fig. 5) will require more investigations along with GPR studies.

8. Conclusions

A renewed interest in LHS for hydrocarbon exploration led us to study its paleostress pattern based on the much less described arc-parallel shear from this terrain. The NW LHS in Uttarakhand (India) experienced two distinct phases of Himalayan arc-parallel deformations: (i) arc-parallel extension (D_{ext}), and (ii) arc-parallel compression (D_{compr}). Paleostress analysis reveals D_{ext} generates an expansion along 131°–311° and D_{compr} a shortening along the same direction (133.5°–313.5°). We could not derive temporal relation between these two phases due to the absence of cross-cut evidences in the field, under an optical microscope and inconclusive geochronologic information available in the literature.

Based on previous studies and this work, we understand that the arc-parallel shear continues from the Indus-Tsangpo Suture Zone (ITSZ) up to the Siwalik range. Thus, arc-parallel deformation is much more ubiquotous in the Himalayan belt than previously discussed. We speculate that the Delhi-Haridwar Ridge (DHR) and the Dehradun lineament played a significant role in modifying the strain, seismicity and deformation pattern within the NW Indian LHS at the upper crustal level.

The study proposes collision-induced crustal overthickening escapes rock masses laterallyresulting in arc-parallel extension. The DHR plausibly indirectly acted as a barrier to the lateral flow, may cause the material to pile up against its wall thereby producing arc-parallel compression. Onset of arc-parallel extension ranged from ~15 to 5 Ma (Stockli et al., 2002; Nagy et al., 2015). NW LHS experienced arc-parallel compression that presumably initiated ~ 4–7 Ma during the NE-SW extension (D_3 of Hintersberger et al., 2011). This can mean that the arc-parallel compression is syn to post-kinematic to the arc-parallel extension. The new structural geological input obtained from this study will be helpful in tectonic modeling of the terrain, and thefore in petroleum geoscience of this terrain.

Authorship contribution statement

Tuhin Biswas: Methodology, Investigation, fieldwork, writing, handling software - original draft, Narayan Bose: Investigation, fieldwork, Dripta Dutta: Writing – review & editing, Soumyajit Mukherjee: Conceptualization, fieldwork, Writing – review & editing.

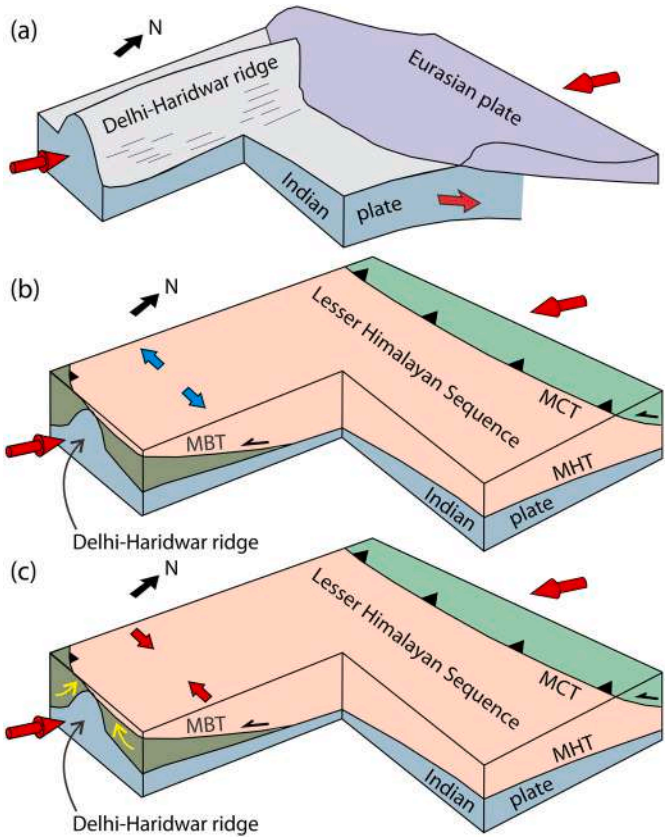

Fig. 17. Block diagrams of the proposed model for the NW LHS, not to scale. (a)Subduction of the Indian plate beneath the Eurasian plate. The Indian plate contains two notable ridges: the Delhi-Haridwar Ridge (DHR) and the Faizabad Ridge as surface highs (Godin and Harris (2014)). Red arrows: compression direction. (b) Scenario 1: Southward propagating thrusts (e.g. MCT, MBT) developed. Elevated portion at the hinge of the DHR exerted arc-parallel, ~ NW-SE trending extension (blue arrows). (c) Scenario 2: Lateral mass flow (blue arrows from 17b) terminated abruptly against the sub-surface elevated ridge, piled up and produces arc-parallel compression (red arrows). MHT: Main Himalayan Thrust.

Declaration of competing interest

Authors declare no conflict of interest with anyone.

Acknowledgements

Part of the Ph.D. thesis of TB. Research Policy Committee members Profs. G.N. Jadhav, P. Naraga and S. Dasgupta (IIT Bombay) provided many critical suggestions. Fieldwork was conducted using IIT Bombay's CPDA grant provided to SM. Associate Editor Tiago Alves and reviewers (Subhobroto Mazumder, Vicor Alania and anonymous) are acknowledged for detail comments in two rounds. Refer to Devi et al. (2022) and Carosi et al. (2022) for updates in Garhwal Himalayan geology and tectonics.

Appendix A

SG2PS: (i) data ID; (ii) group code – 'A' to 'I' is accepted for different set of data from the same location (our data are assigned to the same group); (iii) color code – '0' to '9' can be assigned to plot the groups in different colours; (iv) location details – a minimum of one is required; (v) LOC_X and LOC_Y – coordinates of the locations may or may not be provided; (vi) formation name – not manadatory; (vii) data type – 'striae' for slickenside dataset; (viii) DIP_DIR – dip direction of the Y-plane/C-plane; (viii) DIP – dip amount of the Y-plane/C-plane; (ix) L_DIP_DIR – rake of the slickenline on the fault/shear plane; (x) L_DIP – geographic direction from which rake is calculated; (xii) slip sense – 'up' (reverse slip), 'down' (normal slip); (xi) PALEONORTH – represents previously known north direction (ranging 0°–360°), is left blank; (xii) comments – comments on the data type. We chose Angelier's (1990) inversion technique from the list as the method is able to determine a misfit vector and can correct in between the measured and the calculated shear vector (detail in Sasvári and Baharev, 2014).

T-Tecto: (i) reliability of fault plane data – * (unknown), P (probable), C (certain); (ii) type of fault – N (normal), I (reverse), D (dextral), S (sinistral), ? (unknown); (iii) dip direction of the fault plane; (iv) dip amount of the fault plane; (v) lineation – rake of the slickenline on the fault plane; (vi) direction – geographic direction from which lineation calculated.

Win-Tensor: (i) strike of the fault plane/Y-plane; (ii) dip direction of the fault plane/Y-plane; (iii) rake of slip – '+ve' (reverse slip) and '-ve' for normal slip; (iv) level of certainty – C (certainty), P (probable), S (supposed), X (unknown).

Appendix B

Abbreviations-

GPR:	Ground Penetrating Radar
USGS:	United States Geological Survey
DHR:	Delhi Haridwar Ridge
HHC:	Higher Himalayan Crystalline
ILHS:	Inner Lesser Himalayan Sequence
ISC:	International Seismological Center
LHS:	Lesser Himalayan Sequence
MBT:	Main Boundary Thrust
MCT:	Main Central Thrust
MCT_L:	Lower strand of the Main Central Thrust
MCT_u:	Upper strand of the Mian Central Thrust
MFT:	Main Frontal Thrust
OLHS:	Outer Lesser Himalayan Sequence
THS:	Tethyan Himalayan Sequence
MHT:	Main Himalayan Thrust

REPOSITORY 1

Pre-Himalayan deformation (and metamorphism)

From NW Tethyan Himalayan Muth Formation, microstructural analysis of deformation bands reveals rare evidence of Pre-Himalayan origination. The band orientation indicates N–S stretching and E-W contraction (Draganits et al., 2005). Isoclinal folds in gneiss-migmatite formation are demarcated as Pre-Himalayan orogen product (Jain et al., 2002 and references therein). In Nepal, rare pre-India-Euresian collisional deformation signatures were found in form of Cambrian-Ordovician granite, which cuts through regional folds and foliation, remain younger than garnet-grade regional metamorphism (Bhargava et al., 2011 and references therein). From the Kumaon HHC Himalaya, Patel et al. (2011) identified pre-Himalayan deformation (D_1) along with three Himalayan deformations (D_2, D_3 and D_4). Co-axial reorientation of isoclinal folds (D_1) into NE-plunging folds (D_2) are rare in nature. However, Moharana et al. (2013) suggested the isoclinal folds are product of progressive Himalayan collisional deformation based on the observations within MCT zone (Madlakia-Munsiari Dhapa section, NE Kumaun). During Eocene Eohimalayan phase NW-SE trending isoclinal folds (D_1) presumably resulted due to reactivation of earlier existing structures in THS of western Himalaya (NW India and N Nepal; Aikman et al., 2008). Godin et al. (2019) identified several lineaments trending NW-SE based on Bouguer gravity data belonging to Indian plate extending up to Tibet covered by Himalayan rocks. Analogue centrifuge model predicted the reactivation of such lineaments are capable of producing arc-parallel extension structures on the cover rock.

N–S oriented folds with granite emplacement along axial planar cleavage dated ~1850 Ma ($^{40}Ar/^{39}Ar$ dating of muscovite) in LHS from the Darjeeling-Sikkim Indian Himalaya denotes pre-collisional deformation within the Himalayan orogen (Acharyya et al., 2017). Microstructural study of garnet porphyroblast indicates Paleoproterozoic deformation within LHS (Sikkim Himalaya, Saham 2013). Tripathi et al. (2012) hypothesized a Palaeozoic extensional event (U–Pb geochronology on zircon crystal) based on the magnetic fabrics within Kinnaur Kalish Granite (age: 477.6 ± 3.4 and 472 ± 4 Ma) and associated granites as Pre-Himalayan deformation in South Tibetan Detachment Zone, (Himachal Himalaya, India).

Within the Central Lesser Himalaya, undeformed foliation plane orientation, sedimentary structure and parallel basin sequence indicates the rocks did not underwent any serious Pre-Himalayan deformations (Robinson and McQuarrie, 2012).

U–Pb dating of zircon postulates Bhatwari Gneiss (Garhwal Lesser Himalaya, India) was involved in arc-magmatism in the process of forming Columbia Supercontinent (Sen et al., 2019).

Based on muscovite $^{40}Ar/^{39}Ar$ and K–Ar whole rock cooling age, Oliver et al. (1995) implied pre-Himalayan metamorphism reached up to biotite-grade in the Garhwal Himalaya, whereas, garnet Sm–Nd dating data from Zanskar Himalaya suggests Pre-Himalayan metamorphism rose up to garnet grade (Prince et al., 1994).

REPOSITORY 2

Arc-parallel shear from the Tibet (Fig. 2)

The Thakkhola graben in south Tibet commenced at 14 Ma ($^{40}Ar/^{39}Ar$ dating on mica: Coleman and Hodges, 1995). Around 12–13 Ma is marked as beginning of Kung Co rift extension using the (U–Th)/He thermochronology on zircon and apatite (Lee et al., 2011). From the Gurla Mandhata detachment system in SW Tibet, $^{40}Ar/^{39}Ar$ data from muscovite and biotite suggest 11 Ma as the initiation of arc-parallel extension (Murphy et al., 2002, 2009). $^{40}Ar/^{39}Ar$ thermochronology in the Nyaingentanghla shear zone from southern Tibet reveals arc-parallel extension age to be ~8 Ma (Harrison et al., 1995). Stockli et al. (2002) suggested the onset of extension within the Gulu rift (NE part) in Tibet is ~ 7-5 Ma [apatite (U–Th/He) thermochronology].

REPOSITORY 3

Local structural detail

Based on field observations and cross-cut relations between the structural features, an orthogonal switch in the stress fields trending NE-SW and NW-SE was recorded by the previous authors (e.g., Agarwal and Kumar, 1973; Misra and Bhattacharya, 1973; Jain, 1987; Dubey and Jayangondaperumal, 2005). Agarwal and Kumar (1973) and Misra and Bhattacharya (1973) recorded first phase of deformation resulting NW-SE trending fold later refolded into NE-SW trending doubly plunged folding (second deformation phase). Saklani (1979) and Shekhar et al. (2006) considered folds developed under NW-SE compression are of third deformation phase. Fourth generation of folding trends E-W in Garhwal Lesser Himalaya (Shekhar et al., 2006).

In contrary, Valdiya (1976), Pant et al., (2012) and Sharma and Bhatt (1990) proposed NE-SW trending folds to be of first deformation product. Sharma and Bhatt (1990) proposed an additional arc-parallel folding in ENE-WSW trend as second generation folding. Sharma and Bhatt (1990) noted a third set of folding with axial plane-oriented WNW-ESE in the form of an arc-parallel folding. Saxena (1974) and Sharma and Bhatt (1990) added another set of deformation in the form of NNW-trending folds.

Bagri (2006a) mapped metabasic rocks layer running south of the MCT_L. No sharp contact between the LHS and the HHC is found near Sainj since the MCT_L is covered by landslide materials, which connotes the active nature of the MCT_L (Bagri, 2006a). Two sets of joints are found from the Uttarkashi area, with one striking ~40°NE and the other 130°-140°SE (Bagri, 2006b).

Three deformation phases have been worked out in field from Purola near Uttrakashi of unknown timing. These are D1: S1 foliation development; D2: S2 foliation development and flexure slip folding; D3: refolding of veins and chevron folding (Pachauri, 2005). Bhatt and Saklani (1990) showed in micro-scale that the quartz grains in the Pratapnagar thrust sheet (=Berinag/Dunda thrust), the Pratapnagar quartzite (=Berinag quartzite) are stretched along ~ NE-SW and underwent progressive plane and constrictional strain. Bhatt and Saklani (1994) further show that rocks on the Pratapnagar thrust were dominantly simple sheared and bear lineations plunging $10\text{-}25^0$, whereas those away from the thrust were pure sheared. The Pratapnagar Thrust shows both brittle and ductile shear evidences (Bhatt and Saklani, 1994). Dunda Thrust and Singauni Thrust show opposite sense of shears (Bhatt, 1996). From Garhwal Himalaya structures locally show significant variations. For example, the thrust sheets have been affected by four phases of deformation. These are D1: coaxial F1 and F2 folding, F3 folding during D2 shear, and D3 and D4 produced F4 folding and transverse faults, respectively (Bhatt, 1996). Saklani (1979) reported NW and SE dip direction of schistosity of the Mukhem Schist.

Pandey et al. (2005) identified ~ NE-SW trending 1096 lineaments within the Tehri-Uttarkashi District in the LHS. Landsat images reveal several major lineaments within the Garhwal Lesser Himalaya viz., the Nagaon Lineament that trends 130°– 310° parallels the Tons Thrust for 110 km, the 170°– 350° trending Tehri Lineament, which continues for ~180 km from the Indo-Gangetic plane up to the MCT and across both the ILHS and OLHS (Bharktya and Gupta, 1982). Geomorphic studies by Pandey et al. (2005) reveal five phases of uplift in the Tehri-Uttarkashi region. However, timings of these uplift have stayed unconstrained. From Tehri District Mangain et al. (2012) reported N–S trending anticline.

In Tehri dam foundation, the main foliation dips ~ S. Here several shear planes were traced that are either longitudinal or diagonal to the foliation plane (Nawani and Sanwal, 1996).

Several younger steep faults cut across older thrusts e.g., the Ramgarh Thrust cuts the MCT. Such younger thrusts are the out-of-sequence thrusts (review in Mukherjee, 2015).

Around 6 mm y^{-1} arc normal extension from Tethyan NW Himalaya was estimated by Jade et al. (2014) and correlated with the E-W Tibetan extension.

REPOSITORY 4

Landslides

Barnard et al. (2001) predicted ~ 66% of the landslides within the Garhwal Himalaya are initiated due to increase in human interference (e.g. road construction). Heavy construction works involving landslides lead earthquakes in the past (e.g., Kashmir earthquake, 2005; Owen et al., 2008). Kumar and Anbalagan (2016) pointed out reservoir water fluctuation area to be one of the major factors for the increased frequency of landslide around Tehri reservoir. Bagri (2006b) suggested, movement of Delhi-Haridwar Ridge in response with Indian plate movement triggers the rock mass slumping. The 23-Sept-2003 Varunavat landslide, one of the significant landslides within Garhwal Himalaya, was due to heavy rainfall (Sarkar et al., 2011).

Type of rocks and geologically structure contributes 72% of the landslides occurring within Garhwal Himalaya (Naithani, 2007). Greywackes, siltstone, phyllites, limestones and slates are more prone to landslides within Garhwal Himalaya (Pareek et al., 2013). Rautgara Formations are more prone to landslides (Nair and Singh, 2020), whereas Kumar and Anbalagan (2016) pointed out that the Blaini and the Rautgara formation are stable in terms of landslide susceptibility, whereas the Chandpur Formation is highly vulnerable. Mithal (1988) considered that the joint planes and foliation planes with less vegetation made Krol limestone and Nagthat quartzite more landslide prone, compare to rocks of higher metamorphic grade or massive in nature (massive Krol limestone). Saha et al. (2002) suggested bivariate statistical method to be useful in marking regional scale landslide zone, dealing with landslide prone area along structural weak zones, dividing smaller areas from very low to very high susceptibility zones. Repositories 6 and 7 present landslides documented in this study.

REPOSITORY 5

Fundamentals and principles involved in the paleostress studies

Paleostress analysis was introduced in 1970s to decode past stress regimes based on brittle plane data (e.g., Carey and Brunier, 1974). The stress inversion method relies on a few basic assumptions (reviewed in Vanik et al., 2018; Shaikh et al., 2020): (i) stress field under which brittle deformation took place should be homogeneous; (ii) all slip data (attitudes of fault planes and that of the slip lineations) are the product of a single deformation, therefore to run paleostress analysis, manual segregation of heterogenous data set into homogenous subset provides a better control (Kounov, 2011); (iii) deformation does not involve block rotation; (iv) slips along separate fault planes are mutually independent; (v) displacement is small compared to the size of the fault; and (vi) resolved maximum shear stress direction parallels the direction of slip.

The software Structural Geology to Post Script (SG2PS) version 2 (Sasvári and Baharev, 2014) compiles seven paleostress inversion algorithms

contributed by various authors into a single software. The software offers a range of different paleostress methods e.g., Turner (1953), Spang (1972), Michael (1984), Angelier (1990), Fry (1999), Shan et al. (2004), and Mostafa et al. (2005). Field dataset can be run using any of these methods – the choice lies with the user. Apart from determining the orientation of principal stress axes, the software also runs Bingham statistics, which calculates the arithmetic average of a processed dataset to produce directional distribution of fractures by generating a density ellipsoid in which the principal stress axes directions are modified as maximum, intermediate and minimum density directions. The distribution geometry are denoted by the axes length of the density ellipsoid.

The T-TECTO version X5 is a paleostress software (Žalohar and Vrabec, 2007) that applies the Gauss numerical method to perform the inversion operation. Apart from the Right Dihedra Method (RDM), it also provides Visualization of the Gauss Function Method (VGF Method: Žalohar and Vrabec, 2007). This yields a statistical averaged solution for the orientation of principle stress axes and stress ratio (a ratio between normal stress and shear stress on the slip-plane). The VGF method can be utilized for different type of fault planes (Vanik et al., 2018), and additionally all types of fracture planes without visible slip (Dutta et al., 2019).

The Win-Tensor version 5.8.8 paleostress analysis software (Delvaux and Sperner, 2003) utilizes Angelier's paleostress reconstruction method (Angelier, 1989, 1994) to calculate the optimum reduced stress axes. The software provides an improved version of graphical Right Dihedral Method (RDM). Here the direction of resolved stress axes for each fault plane are averaged out to derive the orientation of three principle stress axes and relative magnitude of principal stress axes (default value of $\sigma_1 = 100$, $\sigma_3 = 0$; $\sigma_3 \leq \sigma_2 \leq \sigma_1$). Slip sense along the fault has to be provided by the user as an input. Therefore, correctly deciphering the same in the field is crucial. The improved RDM version provides a stress ratio {$R = (\sigma_2 - \sigma_3)/(\sigma_1 - \sigma_3)$} and recognizes the stress regime as well. A counting deviation is an additional function by which misfit data gets eliminated from a heavily populated dataset.

Caption for Repository 6 & 7:

Repository 6

Landslides producing debris flow from the Garhwal Lesser Himalaya. Debris material contains soil and rock fragments (up to boulder size). (a) in MCT zone schists and quartzites at 30.8136° N, 78.6205° E, Location 1 also known as Lata ghatori slide in Fig. 5. (b) At Munsiari Thust footwall at 30.7725° N, 78.5997° E, Location 6 in Fig. 5. (c) Within Berinag Formation quartzites at 30.76° N, 78.5811° E, at location 8 in Fig. 5. (d) within quartzites of Berinag Formation at 30.7544° N, 78.5593° E, near location 4 in Fig. 5, also known as Ganeshpur slide.

Repository 7

Boulder size rock particles avalanching within Garhwal Lesser Himalaya. Debris material contains soil and rock fragments. (a) Within Berinag Formation quartzites at 30.7432° N, 78.3586° E, Location 25 in Fig. 5 also known as Raturi sear slide. S. Mukherjee (height ~ 165 cm) as the marker. (b) In Berinag Formation quartzites at 30.6802° N, 78.3497° E, south of location 29 in Fig. 5, marked as 'k: unnamed' also reported by Nair and Singh (2020). (c) within Rautgara Formation quartzites at 30.6599° N, 78.3364° E, marked as 'l: unnamed' in Fig. 5, also reported by Nair and Singh (2020). (d) In quartzites of Rautgara Formation at 30.6517° N, 78.3322° E, marked as 'm: unnamed' in Fig. 5, also reported by Nair and Singh (2020).

Appendix C. Supplementary data

Supplementary data related to this article can be found at https://doi.org/10.1016/j.marpetgeo.2022.105530.

References

Acharyya, S.K., Ghosh, S., Mandal, N., Bose, S., Pande, K., 2017. Pre-Himalayan tectono-magmatic imprints in the Darjeeling-Sikkim Himalaya (DSH) constrained by 40Ar/39Ar dating of muscovite. J. Asian Earth Sci. 146, 211–220.

Agarwal, N.C., Kumar, G., 1973. Geology of the upper Bhagirathi and yamuna valleys, Uttarkashi District, Kumaun Himalaya. Himal. Geol. 3, 1–23.

Agarwal, A., Agarwal, K.K., Bali, R., Prakash, C., Joshi, G., 2016. Back-thrusting in Lesser Himalaya: evidences from magnetic fabric studies in parts of Almora Crystalline Zone, Kumaun Lesser Himalaya. J. Earth Syst. Sci. 125, 873–884.

Ahmad, T., Harris, N., Bickle, M., Chapman, H., Bunbury, J., Prince, C., 2000. Isotopic constraints on the structural relationships between the lesser Himalayan series and the high Himalayan crystalline series, Garhwal Himalaya. Geol. Soc. Am. Bull. 112 (3), 467–477.

Aikman, A.B., Harrison, T.M., Lin, D., 2008. Evidence for early (> 44 Ma) himalayan crustal thickening, tethyan Himalaya, southeastern Tibet. Earth Planet Sci. Lett. 274 (1–2), 14–23.

Allmendinger, R.W., González, G., Yu, J., Hoke, G., Isacks, B., 2005. Trench-parallel shortening in the Northern Chilean Forearc: tectonic and climatic implications. Geol. Soc. Am. Bull. 117, 89–104.

Angelier, J., 1989. From orientation to magnitudes in paleostress determinations using fault slip data. J. Struct. Geol. 11 (1–2), 37–50.

Angelier, J., 1990. Inversion of field data in fault tectonics to obtain the regional stress—III. A new rapid direct inversion method by analytical means. Geophys. J. Int. 103 (2), 363–376.

Angelier, J., 1994. Fault slip analysis and paleostress reconstruction. Continental deformation 53–100.

Ansdell, K.M., Lucas, S.B., Connors, K., Stern, R.A., 1995. Kisseynew metasedimentary gneiss belt, Trans-Hudson orogen (Canada): back-arc origin and collisional inversion. Geology 23 (11), 1039–1043.

Aoya, M., Wallis, S.R., Terada, K., Lee, J., Kawakami, T., Wang, Y., Heizler, M., 2005. North-south extension in the Tibetan crust triggered by granite emplacement. Geology 33 (11), 853–856.

Armijo, R., Tapponnier, P., Mercier, J.L., Han, T.L., 1986. Quaternary extension in southern Tibet: field observations and tectonic implications. J. Geophys. Res. Solid Earth 91 (B14), 13803–13872.

Arora, B.R., Gahalaut, V.K., Kumar, N., 2012. Structural control on along-strike variation in the seismicity of the northwest Himalaya. J. Asian Earth Sci. 57, 15–24.

Avé Lallemant, H.G., Guth, L.R., 1990. Role of extensional tectonics in exhumation of eclogites and blueschists in an oblique subduction setting: northeastern Venezuela. Geology 18 (10), 950–953.

Azmi, R.J., 1981. Microfauna and age of the lower tal phosphorite of Mussoorie Syncline, garhwal lesser Himalaya. Himal. Geol. 11 (1981 Pg), 373–409.

Bagri, D.S., 2006a. The natural hazards in Uttarakashi and Tehri districts, Uttaranchal Himalaya. In: Saklani, P.S. (Ed.), Himalaya (Geological Aspects) 4th Volume Satish, vol. 91. Serial Publishing House, New Delhi, ISBN 81-89304-14-3, p. 106.

Bagri, D.S., 2006b. The Varunavat landslide in Uttarkashi. In: Dhasmana, R.P., Dhoundiyal, V.L. (Eds.), Uttarakhand: Need for a Comprehensive Eco-Strategy 131-134. V.K. Publishers, New Delhi.

Barnard, P.L., Owen, L.A., Sharma, M.C., Finkel, R.C., 2001. Natural and human-induced landsliding in the Garhwal Himalaya of northern India. Geomorphology 40 (1–2), 21–35.

Bhambri, R., Mehta, M., Singh, S., Jayangondaperumal, R., Gupta, A.K., Srivastava, P., 2017. Landslide inventory and damage assessment in the Bhagirathi valley, Uttarakhand, during June 2013 flood. Himal. Geol. 38, 193–224.

Bhargava, O.N., Frank, W., Bertle, R., 2011. Late cambrian deformation in the lesser Himalaya. J. Asian Earth Sci. 40 (1), 201–212.

Bhatt, S.C., 1996. In: Proceedings Symposium on Recent Advances in Geological Studies of Northwest Himalaya and the Foredeep, vol. 2. Special Publication 21, Lucknow, pp. 45–52.

Bhatt, S.C., Saklani, P.S., 1990. Kinematic framework of heterogeneous deformation within pratapnagar thrust sheet, Bhagirathi valley, in lesser garhwal Himalaya, U.P. J. Geol. Soc. India 36, 247–261.

Bhatt, S.C., Saklani, P.S., 1994. Strain transition and microstructural-fabric analysis of quartz mylonites exposed within Pratapnagar nappe, Garhwal Himalaya, India. J. Geol. Soc. India 43, 381–394.

Bhattacharya AR. (Internet reference) Himalayan deformation: implications for hydrocarbon exploration. URL: file:///C:/Users/Guest/Downloads/lecture-technicaldetails% 20(2).pdf (Accessed on 25-May-2019).
Boccaletti, M., Sani, F., 1998. Cover Thrust reactivations related to internal basement involvement during Neogene-Quaternary evolution of the Northern Apennines. Tectonics 17 (1), 112–130.
Bollinger, L., Avouac, J.P., Cattin, R., Pandey, M.R., 2004. Stress buildup in the Himalaya. J. Geophys. Res. Solid Earth 109 (B11).
Bonini, M., Sokoutis, D., Talbot, C.J., Boccaletti, M., Milnes, A.G., 1999. Indenter growth in analogue models of Alpine-type deformation. Tectonics 18 (1), 119–128.
Bose, N., Mukherjee, S., 2019a. Field documentation and genesis of the back-structures from the garhwal lesser Himalaya, Uttarakhand, India. In: Sharma, R., Villa, I.M., Kumar, S. (Eds.), Crustal Architecture and Evolution of the Himalaya-Karakoram-Tibet Orogen, vol. 481. Geological Society of London Special Publications, pp. 111–125.
Bose, N., Mukherjee, S., 2019b. Field documentation and genesis of back-structures in ductile and brittle regimes from the foreland part of a collisional orogen: examples from the Darjeeling–Sikkim Lesser Himalaya, India. Int. J. Earth Sci. 108, 1333–1350.
Bose, N., Mukherjee, S., 2020. Estimation of deformation temperatures, flow stresses and strain rates from an intra-continental shear zone: the Main Boundary Thrust, NW Himalaya (Uttarakhand, India). Mar. Petrol. Geol. 112, 104094.
Boutelier, D.A., Oncken, O., 2010. Role of the plate margin curvature in the plateau buildup: consequences for the central Andes. J. Geophys. Res. Solid Earth 115 (B4).
Bradshaw, J.D., Weaver, S.D., Muir, R.J., 1996. Mid-Cretaceous oroclinal bending of New Zealand terranes. N. Z. J. Geol. Geophys. 39 (3), 461–468.
Brown, D., Alvarez-Marron, J., Perez-Estaun, A., Puchkov, V., Ayala, C., 1999. Basement influence on foreland thrust and fold belt development: an example from the southern Urals. Tectonophysics 308 (4), 459–472.
Burg, J.P., Nievergelt, P., Oberli, F., Seward, D., Davy, P., Maurin, J.C., Diao, Z., Meier, M., 1998. The Namche Barwa syntaxis: evidence for exhumation related to compressional crustal folding. J. Asian Earth Sci. 16 (2), 239–252.
Carey, S.W., 1955. The orocline concept in geotectonics-Part I. Papers and Proceedings of the Royal Society of Tasmania vol. 89, 255–288.
Carey, E., Brunier, B., 1974. Analyse théorique et numérique d'un modèlemécaniqueélémentaire appliqué à l'étuded'une population de failles: calcul d'un tenseurmoyen de contraintes à partir des stries de glissement. ComptesRendus de l'Académie des Sciences Paris D 279, 891–894.
Carosi, R., Montomoli, C., Pertusati, P.C., 2004. Late tectonic evolution of the Northern Apennines: the role of contractional tectonics in the exhumation of the Tuscan units. Geodin. Acta 17 (4), 253–273.
Catalán, J.R.M., Pascual, F.J.R., Montes, A.D., Fernández, R.D., Barreiro, J.G., Da Silva, Í. D., Clavijo, E.G., Ayarza, P., Alcock, J.E., 2014. The late Variscan HT/LP metamorphic event in NW and Central Iberia: relationships to crustal thickening, extension, orocline development and crustal evolution. In: Schulmann, K., Martínez Catalán, J.R., Lardeaux, J.M., Janoušek, V., Oggiano, G. (Eds.), 2014. The Variscan Orogeny: extent, Timescale and the Formation of the European Crust. Geological Society, London, Special Publications 405, pp. 225–247.
Catlos, E. J., Perez, T., Lovera, O., Dubey, C. S., Schmitt, A. K., & Etzel, T. M. High-resolution P-T-time paths across Himalayan faults exposed along the Bhagirathi Transect NW India: implications for the construction of the Himalayan orogen and ongoing deformation. G-cubed, e2020GC009353.
Catlos, E.J., Harrison, T.M., Manning, C.E., Grove, M., Rai, S.M., Hubbard, M.S., Upreti, B.N., 2002. Records of the evolution of the Himalayan orogen from in situ Th–Pb ion microprobe dating of monazite: eastern Nepal and western Garhwal. J. Asian Earth Sci. 20, 459–479.
Célérier, J., Harrison, T.M., Webb, A.A.G., Yin, A., 2009. The Kumaun and garwhal lesser Himalaya, India: Part 1. Structure and stratigraphyTheKumaun and garwhal lesser Himalaya: structure and stratigraphy. GSA Bulletin 121 (9–10), 1262–1280.
Chakroborty, S.K., Malaviya, A.K., 1995. Geology of the Almora Gorup of Kumaon Lesser Himalaya. Geol. Surv. India Spl. Publ. 21, 39–45.
Coleman, M., Hodges, K., 1995. Evidence for Tibetan plateau uplift before 14 Myr ago from a new minimum age for east–west extension. Nature 374 (6517), 49–52.
Colleps, C.L., Stockli, D.F., McKenzie, N.R., Webb, A.A.G., Horton, B.K., 2019. Neogene kinematic evolution and exhumation of the NW India Himalaya: zircon geoand thermochronometric insights from the fold-thrust belt and foreland basin. Tectonics 38, 2059–2086.
Cooper, M., 2007. Structural style and hydrocarbon prospectivity in fold and thrust belts: a global review. In: Ries, A.C., Butler, R.W.H., Graham, R.H. (Eds.), Deformation of the Continental Crust: the Legacy of Mike Coward, vol. 272. Geological Society, London, Special Publications, pp. 447–472.
Copley, A., Avouac, J.P., Royer, J.Y., 2010. India-Asia collision and the Cenozoic slowdown of the Indian plate: implications for the forces driving plate motions. J. Geophys. Res. Solid Earth 115 (B3).
Craig, J., Hakhoo, N., Hafiz, M., Khan, M.R., Misra, R., Pandita, S.K., Raina, B.K., Thurow, J., Thusu, B., Ahmed, W., Khullar, S., 2018. Petroleum systems and hydrocarbon potential of the North-West Himalaya of India and Pakistan. Earth Sci. Rev. 187, 109–185.
Dalmayrac, B., Molnar, P., 1981. Parallel thrust and normal faulting in Peru and constraints on the state of stress. Earth Planet Sci. Lett. 55 (3), 473–481.
Dal Zilio, L., Jolivet, R., Dinther, Y van, 2022. Geophys. Res. Lett. 47, e2019GRL086424.
Davis, B.K., Maidens, E., 2003. Archaean orogen-parallel extension: evidence from the northern eastern goldfields province, Yilgarn craton. Precambrian Res. 127 (1–3), 229–248.
DeCelles, P.G., Robinson, D.M., Quade, J., Ojha, T.P., Garzione, C.N., Copeland, P., Upreti, B.N., 2001. Stratigraphy, structure, and tectonic evolution of the Himalayan fold-thrust belt in western Nepal. Tectonics 20 (4), 487–509.
Delvaux, D., Sperner, B., 2003. New aspects of tectonic stress inversion with reference to the TENSOR program. Geological Society, London, Special Publications 212 (1), 75–100.
Dilek, Y., Altunkaynak, Ş., 2007. Cenozoic crustal evolution and mantle dynamics of post-collisional magmatism in western Anatolia. Int. Geol. Rev. 49 (5), 431–453.
Draganits, E., Grasemann, B., Hager, C., 2005. Conjugate, cataclastic deformation bands in the Lower Devonian Muth Formation (Tethyan Zone, NW India): evidence for pre-Himalayan deformation structures. Geol. Mag. 142 (6), 765–781.
Dubey, A.K., 2014. Understanding an Orogenic Bel. Springer, Heidelberg, New York, Dordrecht, London.
Dubey, A.K., Jayangondaperumal, R., 2005. Pop-up klippen in the Mussoorie Syncline Lesser Himalaya: evidence from field and model deformation studies. In: Saklani, P. S. (Ed.), Himalaya (Geological Aspects), vol. 3. Satish Serial Publishing House, Delhi, pp. 203–222.
Dutta, D., Mukherjee, S., 2019. Opposite shear senses: geneses, global occurrences, numerical simulations and a case study from the Indian western Himalaya. J. Struct. Geol. 126, 357–392.
Dutta, D., Mukherjee, S., 2021. Extrusion kinematics of UHP terrane in a collisional orogen: EBSD and microstructure-based approach from the Tso Morari Crystallines (Ladakh Himalaya). Tectonophysics 800, 228641.
Dutta, D., Biswas, T., Mukherjee, S., 2019. Arc-parallel compression in the NW Himalaya: evidence from structural and palaeostress studies of brittle deformation from the clasts of the Upper Siwalik, Uttarakhand, India. J. Earth Syst. Sci. 128 (5), 125.
Ellis, M., Watkinson, A.J., 1987. Orogen-parallel extension and oblique tectonics: the relation between stretching lineations and relative plate motions. Geology 15 (11), 1022–1026.
England, P., Houseman, G., 1989. Extension during continental convergence, with application to the Tibetan Plateau. J. Geophys. Res. Solid Earth 94 (B12), 17561–17579.
England, P.C., Richardson, S.W., 1977. The influence of erosion upon the mineral fades of rocks from different metamorphic environments. J. Geol. Soc. 134 (2), 201–213.
Faure, M., 1995. Late orogenic carboniferous extensions in the variscan French massif central. Tectonics 14 (1), 132–153.
Frisch, W., Dunkl, I., Kuhlemann, J., 2000. Post-collisional orogen-parallel large-scale extension in the Eastern Alps. Tectonophysics 327 (3–4), 239–265.
Fry, N., 1999. Striated faults: visual appreciation of their constraint on possible paleostress tensors. J. Struct. Geol. 21 (1), 7–21.
Gahalaut, V.K., Kundu, B., 2012. Possible influence of subducting ridges on the Himalayan arc and on the ruptures of great and major Himalayan earthquakes. Gondwana Res. 21 (4), 1080–1088.
Gansser, A., 1964. Geology of the Himalayas. Wiley InterScience, New York.
Gautam, P.K., Gahalaut, V.K., Prajapati, S.K., Kumar, N., Yadav, R.K., Rana, N., Dabral, C.P., 2017. Continuous GPS measurements of crustal deformation in Garhwal-Kumaun Himalaya. Quat. Int. 462, 124–129.
Gelabert, B., Sàbat, F., Rodríguez-Perea, A., 2002. A new proposal for the late Cenozoic geodynamic evolution of the western Mediterranean. Terra. Nova 14 (2), 93–100.
Ghosh, R., Mukherjee, 2021. Structural geology of Lesser Himalaya in and around an out-of-sequence thrust in the Chaura area (Himachal Pradesh, India). In: Mukherjee, S. (Ed.), Structural Geology and Tectonics Field Guidebook – Volume 1. Springer Nature Switzerland AG, ISBN 978-3-030-60143-0, pp. 413–428.
Godin, L., Harris, L.B., 2014. Tracking basement cross-strike discontinuities in the Indian crust beneath the Himalayan orogen using gravity data–relationship to upper crustal faults. Geophys. J. Int. 198 (1), 198–215.
Godin, L., Gleeson, T.P., Searle, M.P., Ullrich, T.D., Parrish, R.R., 2006. Locking of southward extrusion in favour of rapid crustal-scale buckling of the Greater Himalayan sequence, Nar valley, central Nepal. Geological Society, London, Special Publications 268 (1), 269–292.
Godin, L., La Roche, R.S., Waffle, L., Harris, L.B., 2019. Influence of inherited Indian basement faults on the evolution of the Himalayan Orogen. Geological Society, London, Special Publications 481 (1), 251–276.
Goffey, G.P., Craig, J., Needham, T., Scott, R., 2010. Fold–thrust belts: overlooked provinces or justifiably avoided?. In: Goffey, G.P., Craig, J., Needham, T., Scott, R. (Eds.), Hydrocarbons in Contractional Belts, vol. 348. Geological Society, London, Special Publications. https://doi.org/10.1144/SP348.0, 2010.
Goswami, P.K., 2012. Geomorphic evidences of active faulting in the northwestern Ganga Plain, India: implications for the impact of basement structures. Geosci. J. 16 (3), 289–299.
Gupta, V., Bhasin, R.K., Kaynia, A.M., Kumar, V., Saini, A.S., Tandon, R.S., Pabst, T., 2016. Finite element analysis of failed slope by shear strength reduction technique: a case study for Surabhi Resort Landslide, Mussoorie township, Garhwal Himalaya. Geomatics, Nat. Hazards Risk 7 (5), 1677–1690.
Hammerstein, J.A., Dicuia, R., Cottam, M.A., Zamora, G., Butler, R.W.H., 2020. Fold and thrust belts: structural style, evolutionand exploration–an introduction. In: Hammerstein, J.A., Dicuia, R., Cottam, M.A., Zamora, G., Butler, R.W.H. (Eds.), Fold and Thrust Belts:Structural Style, Evolution and Exploration, vol. 490. Geological Society, London, Special Publications, pp. 1–8.
Hetzel, R., Ring, U., Akal, C., Troesch, M., 1995. Miocene NNE-directed extensional unroofing in the Menderes Massif, southwestern Turkey. J. Geol. Soc. 152 (4), 639–654.
Hintersberger, E., Thiede, R.C., Strecker, M.R., 2011. The role of extension during brittle deformation within the NW Indian Himalaya. Tectonics 30 (3).
Hodges, K.V., Hurtado, J.M., Whipple, K.X., 2001. Southward extrusion of Tibetan crust and its effect on Himalayan tectonics. Tectonics 20 (6), 799–809.

Hoke, L., Lamb, S., Hilton, D.R., Poreda, R.J., 2000. Southern limit of mantle-derived geothermal helium emissions in Tibet: implications for lithospheric structure. Earth Planet Sci. Lett. 180 (3–4), 297–308.
Iaccarino, S., Montomoli, C., Montemagni, C., Massonne, H.-J., Langone, A., Jain, A.K., Visona, D., Carosi, R., 2020. The Main Central Thrust zone along the Alaknanda and Dhauli Ganga valleys (Garhwal Himalaya, NW India): Insights into an inverted metamorphic sequence. Lithos 372-373, 105669.
Jade, S., Mukul, M., Gaur, V.K., Kumar, K., Shrungeshwar, T.S., Satyal, G.S., Dumka, R. K., Jagannathan, S., Ananda, M.B., Kumar, P.D., Banerjee, S., 2014. Contemporary deformation in the kashmir–himachal, garhwal and Kumaon Himalaya: significant insights from 1995–2008 GPS time series. J. Geodes. 88 (6), 539–557.
Jain, A.K., 1971. Stratigraphy and tectonics of lesser himalayan region of Uttarkashi, garhwal Himalaya. Himal. Geol. 1, 25–58.
Jain, A.K., 1975. Structure and petrology of mylonite and related rocks from the Lesser Himalaya, Garhwal, India. Geol. Rundsch. 64 (1), 230–248.
Jain, A.K., 1987. Kinematics of the transverse lineaments, regional tectonics and Holocene stress field in the Garhwal Himalaya. J. Geol. Soc. India 30, 169–186.
Jain, A.K., Varadaraj, N., 1978. Stratigraphy and provenance of late palaeozoic diamictites in parts of garhwal lesser Himalaya, India. Geol. Rundsch. 67 (1), 49–72.
Jain, A.K., Banerjee, D.M., Mithal, R.S., 1971. Correlation of unfossiliferous lesser himalayan formations of garhwal. Himal. Geol. 1, 92–110.
Jain, A.K., Sing, S., Manickavasagam, R.M., 2002. Himalayan Collision Tectonics. Gondawana Research Group Memoir, vol. 7. Field Science Publishers, Hashimoto, pp. 1–114, 4-938925-13-3-C3344.
Johnston, S.T., Weil, A.B., Gutiérrez-Alonso, G., 2013. Oroclines: thick and thin. Bulletin 125 (5–6), 643–663.
Jolivet, L., De Lamotte, D.F., Mascle, A., Séranne, M., 1999. The Mediterranean basins: Tertiary extension within the Alpine orogen—an introduction. In: Durand, B., Joliver, L., Horvath, F., Seranne, M. (Eds.), The Mediterranean Basins: Tertiary Extension within the Alpine Orogen, vol. 156. Geological Society, London, Special Publications, pp. 1–14.
Joshi, A., Shinval, A., Shinval, H., 1999. A strong motion model for the Uttarkashi earthquake of October 20, 1991. In: Jain, A.K., Manickavasagam, R.M. (Eds.), Geodynamics of the NW Himalaya, vol. 6. Gondwana Research Group Memoir, pp. 335–340.
Joshi, V., Murthy, T.V.R., Arya, A.S., Narayana, A., Naithani, A.K., Garg, J.K., 2003. Landslide hazard zonation of Dharasu-Tehri-Ghansali area of Garhwal Himalaya, India using remote sensing and GIS techniques. J. Nepal Geol. Soc. 28, 85–94.
Ju, W., Wang, J., Fang, H., Gong, Y., Zhang, S., 2017. Paleostress reconstructions and stress regimes in the Nanchuan region of Sichuan Basin, South China: implications for hydrocarbon exploration. Geosci. J. 21, 553–564.
Kanaujia, J., Kumar, A., Gupta, S.C., 2016. Three-dimensional velocity structure around Tehri region of the Garhwal Lesser Himalaya: constraints on geometry of the underthrusting Indian plate. Geophys. J. Int. 205 (2), 900–914.
Kanaujia, J., Mitra, S., Gupta, S.C., Sharma, M.L., 2019. Crustal anisotropy from shear-wave splitting of local earthquakes in the Garhwal Lesser Himalaya. Geophys. J. Int. 219 (3), 2013–2033.
Kapp, P., Guynn, J.H., 2004. Indian punch rifts Tibet. Geology 32 (11), 993–996.
Kapp, P., Yin, A., 2001. Unbending of lithosphere as a mechanism for active rifting in Tibet: insight from elastic modeling. AGU Fall Meeting Abstracts T11E–893, 2001.
Kayal, J.R., Nath, S.K., Goswami, T.R., Roy, S., Ram, S., Srirama, B.V., 2002. Site response study by shear-wave spectral analysis using the 1999 Chamoli earthquake sequence in Garhwal Himalaya. Himal. Geol. 23, 45–50.
Kellett, D.A., Cottle, J.M., Larson, K.P., 2019. The South Tibetan Detachment System: history, advances,definition and future directions. In: Treloar, P.J., Searle, M.P. (Eds.), Himalayan Tectonics: A Modern Synthesis, vol. 483. Geological Society, London, Special Publications, pp. 377–400.
Khattri, K.N., 1992. Local Seismic Investigations in the Garhwal-Kumaon Himalaya, vol. 23. Memoir Geological Society of India, pp. 45–66.
Khattri, K.N., Zeng, Y., Anderson, J.G., Brune, J., 1994. Inversion of strong motion waveforms for source slip function of 1991 Uttarkashi earthquake, Himalaya. J. Himal. Geol. 5, 163–191.
Kleinspehn, K.L., Pershing, J., Teyssier, C., 1989. Paleostress stratigraphy: a new technique for analyzing tectonic control on sedimentary-basin subsidence. Geology 17, 253–256.
Klootwijk, C.T., Conaghan, P.J., Powell, C.M., 1985. The Himalayan Arc: large-scale continental subduction, oroclinal bending and back-arc spreading. Earth Planet Sci. Lett. 75 (2–3), 167–183.
Klootwijk, C.T., Gee, J.S., Peirce, J.W., Smith, G.M., McFadden, P.L., 1992. An early India-Asia contact: paleomagnetic constraints from Ninetyeast ridge, ODP Leg 121. Geology 20 (5), 395–398.
Kounov, A., Burg, J.P., Bernoulli, D., Seward, D., Ivanov, Z., Dimov, D., Gerdjikov, I., 2011. Paleostress analysis of Cenozoic faulting in the Kraishte area, SW Bulgaria. J. Struct. Geol. 33 (5), 859–874.
Kulikowski, D., Amrouch, K., 2018. 4D modelling of fault reactivation using complete paleostress tensors from the Cooper–Eromanga Basin, Australia. Aust. J. Earth Sci. 65, 661–681.
Kumar, R., Anbalagan, R., 2016. Landslide susceptibility mapping using analytical hierarchy process (AHP) in Tehri reservoir rim region, Uttarakhand. J. Geol. Soc. India 87 (3), 271–286.
Kumar, G., Dhaundiyal, J.N., 1979. Stratigraphy and structure of "Garhwal synform'' garhwal and Tehri garhwal districts, Uttar Pradesh. A reappraisal. Himal. Geol. 9 (1), 18–41.
Kumar, G., Dhaundiyal, J.N., 1980. On the stratigraphic position of the Tal Formation, garhwal synform, garhwal and Tehri garhwal districts, Uttar Pradesh. J Paleontol Soc India 23, 58–66.
Kumar, S., Mahajan, A.K., 1994. The Uttarkashi earthquake of 20 October 1991: field observations. Terra. Nova 6 (1), 95–99.
Kumar, M.R., Mishra, D.C., Singh, B., 2013. Lithosphere, crust and basement ridges across Ganga and Indus basins and seismicity along the himalayan front, India and western fold belt, Pakistan. J. Asian Earth Sci. 75, 126–140.
Kundu, B., Yadav, R.K., Bali, B.S., Chowdhury, S., Gahalaut, V.K., 2014. Oblique convergence and slip partitioning in the NW Himalaya: implications from GPS measurements. Tectonics 33 (10), 2013–2024.
Lacombe, O., Bellahsen, N., 2016. Thick-skinned tectonics and basement-involved fold–thrust belts: insights from selected Cenozoic orogens. Geol. Mag. 153 (5–6), 763–810.
Larson, K.P., Ambrose, T.K., Webb, A.A.G., Cottle, J.M., Shrestha, S., 2015. Reconciling Himalayan midcrustal discontinuities: the Main Central thrust system. Earth Planet Sci. Lett. 429, 139–146.
Lee, J., Hacker, B.R., Dinklage, W.S., Wang, Y., Gans, P., Calvert, A., Wan, J.L., Chen, W., Blythe, A.E., McClelland, W., 2000. Evolution of the kangmar dome, southern Tibet: structural, petrologic, and thermochronologic constraints. Tectonics 19 (5), 872–895.
Lee, J., Hacker, B., Wang, Y., 2004. Evolution of North Himalayan gneiss domes: structural and metamorphic studies in Mabja Dome, southern Tibet. J. Struct. Geol. 26 (12), 2297–2316.
Lee, J., Hager, C., Wallis, S.R., Stockli, D.F., Whitehouse, M.J., Aoya, M., Wang, Y., 2011. Middle to late Miocene extremely rapid exhumation and thermal reequilibration in the Kung Co rift, southern Tibet. Tectonics 30, TC2007.
Madin, I.P., Lawrence, R.D., Ur-Rehman, S., 1989. The Northwestern Nanga Parbat–Haramosh Massif: Evidence for Crustal Uplift at the Northwestern Corner of the Indian Craton. Tectonics of the Western Himalayas, vol. 232. Geological Society of America Special Paper, pp. 169–182.
Mandal, S., Robinson, D.M., Kohn, M.J., Khanal, S., Das, O., Bose, S., 2016. Zircon U-Pb ages and Hf isotopes of the Askot klippe, Kumaun, northwest India: implications for Paleoproterozoic tectonics, basin evolution and associated metallogeny of the northern Indian cratonic margin. Tectonics 35 (4), 965–982.
Manglik, A., Kandregula, R.S., Pavankumar, G., 2022. Foreland Basin Geometry and Disposition of Major Thrust Faults as Proxies for Identification of Segmentation along the Himalayan Arc. J. Geol. Soc. India 98, 57–61.
Mantovani, E., Albarello, D., Tamburelli, C., Babbucci, D., Viti, M., 1997. Plate convergence, crustal delamination, extrusion tectonics and minimization of shortening work as main controlling factors of the recent Mediterranean deformation pattern. Ann. Geophys. 40 (3).
Mantovani, E., Albarello, D., Babbucci, D., Tamburelli, C., Viti, M., 2002. Trench-Arc-BackArc systems in the Mediterranean area: examples of extrusion tectonics. J. Virtual Explor. 8, 131–147.
Martin, A.J., 2017. A review of definitions of the himalayan main central thrust. Int. J. Earth Sci. 106 (6), 2131–2145.
Martínez-Díaz, J.J., Hernández-Enrile, J.L., 2004. Neotectonics and morphotectonics of the southern Almería region (Betic Cordillera-Spain) kinematic implications. Int. J. Earth Sci. 93 (2), 189–206.
Martínez-Martínez, J.M., Azañón, J.M., 1997. Mode of extensional tectonics in the southeasternBetics (SE Spain): implications for the tectonic evolution of the peri-Alborán orogenic system. Tectonics 16, 205–225.
Martinod, J., Hatzfeld, D., Brun, J.P., Davy, P., Gautier, P., 2000. Continental collision, gravity spreading, and kinematics of Aegea and Anatolia. Tectonics 19 (2), 290–299.
McCaffrey, R., 1996. Estimates of modern arc-parallel strain rates in fore arcs. Geology 24 (1), 27–30.
McCaffrey, R., Nabelek, J., 1998. Role of oblique convergence in the active deformation of the Himalayas and southern Tibet plateau. Geology 26 (8), 691–694.
Meigs, A.J., Burbank, D.W., Beck, R.A., 1995. Middle-late miocene (> 10 Ma) formation of the main boundary thrust in the western Himalaya. Geology 23, 423–426.
Metcalfe, R.P., 1993. Pressure, temperature and time constraints on metamorphism across the main central thrust zone and high himalayan slab in the garhwal Himalaya. In: Treloar, P.J., Searle, M.P. (Eds.), Himalayan Tectonics, vol. 74. Geological Society London Special Publications, pp. 485–509.
Michael, A.J., 1984. Determination of stress from slip data: faults and folds. J. Geophys. Res. Solid Earth 89 (B13), 11517–11526.
Miller, C.H., Schuster, R., Klötzli, U., Frank, W., Purtscheller, F., 1999. Post-collisional potassic and ultrapotassic magmatism in SW Tibet: geochemical and Sr–Nd–Pb–O isotopic constraints for mantle source characteristics and petrogenesis. J. Petrol. 40 (9), 1399–1424.
Miller, C., Klötzli, U., Frank, W., Thöni, M., Grasemann, B., 2000. Proterozoic crustal evolution in the NW Himalaya (India) as recorded by circa 1.80 Ga mafic and 1.84 Ga granitic magmatism. Precambrian Res. 103 (3–4), 191–206.
Misra, R.C., Bhattacharya, A.R., 1973. A study of the tectonites and rock deformation around Kapkot, Kamaun Himalaya. Himal. Geol. 3, 320–335.
Mishra, P., Mukhopadhyay, D.K., 2012. Structural evolution of the frontal fold–thrust belt, NW Himalayas from sequential restoration of balanced cross-sections and its hydrocarbon potential. Geol. Surv. India Spl. Publ. 366 (1), 201–228.
Mithal, R.S., 1988. Lithotectonic landslides and hazard in parts of garhwal-kumaon Himalaya, 2nd intl. In: Conf. On Case Histories in Geotech. Engg.. St. Louis (USA).
Moharana, A., Mishra, A., Srivastava, D.C., 2013. Deformation style in the Munsiari thrust zone: a study in the madlakia–munsiari–dhapa section in north-eastern Kumaun Himalaya. Int. J. Earth Sci. 102 (7), 1837–1849.
Molnar, P., Tapponnier, P., 1978. Active tectonics of Tibet. J. Geophys. Res. Solid Earth 83 (B11), 5361–5375.
Molnar, P., Lyon-Caent, H., 1989. Fault plane solutions of earthquakes and active tectonics of the Tibetan Plateau and its margins. Geophys. J. Int. 99 (1), 123–153.

Molnar, P., Tapponnier, P., 1975. Cenozoic tectonics of Asia: effects of a continental collision. Science 189 (4201), 419–426.
Molnar, P., Fitch, T.J., Wu, F.T., 1973. Fault plane solutions of shallow earthquakes and contemporary tectonics in Asia. Earth Planet Sci. Lett. 19 (2), 101–112.
Molnar, P., Chen, W.P., Padovani, W.E., 1983. Calculated temperatures in overthrust terrains and possible combinations of heat sources responsible for the Tertiary granites in the Greater Himalaya. J. Geophys. Res.: Solid Earth 88 (B8), 6415–6429.
Montemagni, C., Villa, I.M., 2021. Geochronology of Himalayan Shear Zones: Unravelling the Timing of Thrusting from Structurally Complex Fault Rocks. Journal of the Geological Society (in press).
Montemagni, C., Montomoli, C., Iaccarino, S., Carosi, R., Jain, A.K., Massonne, H.-J., Villa, I.M., 2019. Dating protracted fault activities: microstructures, microchemistry and geochronology of the vaikrita thrust, main central thrust zone, garhwal Himalaya, NW India. In: Sharma, R., Villa, I.M., Kumar, S. (Eds.), Crustal Architecture and Evolution of the Himalaya–Karakoram– Tibet Orogen, vol. 481. Geological Society, London, Special Publications, pp. 127–146, 2019.
Montemagni, C., Carosi, R., Fusi, N., Iaccarino, S., Montomoli, C., Villa, I.M., 2020. Three-dimensional vorticity and time-constrained evolution of the Main Central Thrust zone, Garhwal Himalaya (NW India). Terra. Nova 32, 215–224.
Mostafa, M.S., Barrier, E., Abdel Meguid, A.A., 2005. Paleostress evolution of the northern African margin in Egypt. 7 th Intr. In: Conf., for Geology of the Arab World (GAW), pp. 321–346. Cairo, Egypt.
Mouthereau, F., Lacombe, O., Vergés, J., 2012. Building the Zagros collisional orogen: timing, strain distribution and the dynamics of Arabia/Eurasia plate convergence. Tectonophysics 532, 27–60.
Mukherjee, S., 2015. A review on out-of-sequence deformation in the Himalaya. In: Mukherjee, S., Carosi, R., van der Beek, P., Mukherjee, B.K., Robinson, D. (Eds.), Geological Society, London, Special Publications vol. 412, 67–109, 1 Tectonics of the Himalaya.
Mukhopadhyay, D.K., Mishra, P., 2005. A balanced cross section across the Himalayan frontal fold-thrust belt, Subathu area, Himachal Pradesh, India: thrust sequence, structural evolution and shortening. J. Asian Earth Sciences 25, 735–746.
Murphy, M.A., Copeland, P., 2005. Transtensional deformation in the central Himalaya and its role in accommodating growth of the Himalayan orogen. Tectonics 24 (4).
Murphy, M.A., Yin, A., Kapp, P., Harrison, T.M., Manning, C.E., Ryerson, F.J., Lin, D., Jinghui, G., 2002. Structural evolution of the GurlaMandhata detachment system, southwest Tibet: implications for the eastward extent of the Karakoram fault system. Geol. Soc. Am. Bull. 114, 428–447.
Murphy, M.A., Saylor, J.E., Ding, L., 2009. Late Miocene topographic inversion in southwest Tibet based on integrated paleoelevation reconstructions and structural history. Earth Planet Sci. Lett. 282 (1–4), 1–9.
Nagy, C., Godin, L., Antolín, B., Cottle, J., Archibald, D., 2015. Mid-Miocene initiation of orogen-parallel extension, NW Nepal Himalaya. Lithosphere 7 (5), 483–502.
Nair, A.S., Singh, S.K., 2020. Landslide susceptibility mapping in the dharasu-uttarkashi national Highway NH-108/34, NW Himalaya. Himal. Geol. 41 (1), 81–92.
Naithani, A., 2007. Macro landslide hazard zonation mapping using uni-variate statistical analysis in parts of Garhwal Himalaya. J. Geol. Soc. India 70, 353–368.
Nawani, P.C., Sanwal, R., 1996. Geotechnical assessment of Tehri dam foundation. In: Proceedings Symposium on Recent Advances in Geological Studies of Northwest Himalaya and the Foredeep, vol. 1. Special Publication 21, Lucknow, pp. 73–85.
Negi, J.G., Agrawal, P.K., Thakur, N.K., 1989. Inversion of regional gravity anomalies and main features of the deep crustal geology of India. Tectonophysics 165 (1–4), 155–165.
Nelson, K.D., Zhao, W., Brown, L.D., Kuo, J., Che, J., Liu, X., et al., 1996. Partially molten middle crust beneath southern Tibet: synthesis of project INDEPTH results. Science 274 (5293), 1684–1688.
Neupane, B., Zhao, J., Ju, Y., Baral, U., 2020. Occurrence of unconventional hydrocarbon deposits and its structural relation in Nepal Himalaya: implication for future exploration. Arabian J. Geosci. 13, 81.
Ni, J., Barazangi, M., 1984. Seismotectonics of the Himalayan collision zone: geometry of the underthrusting Indian plate beneath the Himalaya. J. Geophys. Res. Solid Earth 89 (B2), 1147–1163.
Oliver, G.J.H., Johnson, M.R.W., Fallick, A.E., 1995. Age of metamorphism in the Lesser Himalaya and the Main Central Thrust zone, Garhwal India: results of illite crystallinity, 40 Ar–39 Ar fusion and K–Ar studies. Geol. Mag. 132 (2), 139–149.
Owen, L.A., Kamp, U., Khattak, A.G., Harp, E.L., Keefer, D.K., Bauer, M.A., 2008. Landslides triggered by the 8 october 2005 Kashmir earthquake. Geomorphology 94, 1–9.
Özsayin, E., Dirik, K., 2011. The role of oroclinal bending in the structural evolution of the Central Anatolian Plateau: evidence of a regional changeover from shortening to extension. Geol. Carpathica 62 (4), 345–359.
Pachauri, A.K., 2005. Structures of Purola area, garhwal Himalaya. In: Saklani, P.S. (Ed.), Himalaya (Geological Aspects), vol. 2. Satish Serial Publishing House, pp. 171–190, 91-902289-7-8.
Pandey, A.C., Saklani, Dubey, C.S., 2005. Geological and morphotectonic studies using satellite images of a part of tehri-uttarakhashi District, lesser garhwal Himalaya. Himalaya (Geological Aspect) 3, 153–171.
Pareek, N., Pal, S., Sharma, M.L., Arora, M.K., 2013. Study of effect of seismic displacements on landslide susceptibility zonation (LSZ) in Garhwal Himalayan region of India using GIS and remote sensing techniques. Comput. Geosci. 61, 50–63.
Pasari, S., & Arora, S. Earthquake probabilities in the Kumaun-Garhwal Himalaya from stochastic modeling of moderate-to-large seismic events. Int. J. Appl. Nat. Sci. 6, 31-44.
Passchier, C.W., Trouw, R.A.J., 2005. Microtectonics, second ed. Springer, Berlin.
Patel, R.C., Adlakha, V., Singh, P., Kumar, Y., Lal, N., 2011. Geology, structural and exhumation history of the higher himalayan Crystallines in Kumaon Himalaya, India. J. Geol. Soc. India 77 (1), 47–72.
Patel, R.C., Singh, P., Lal, N., 2015. Thrusting and back-thrusting as post-emplacement kinematics of the Almora klippe: Insights from Low-temperature thermochronology. Tectonophysics 653, 41–51.
Paul, A., 2010. Evaluation and implications of seismic events in Garhwal-Kumaun region of Himalaya. J. Geol. Soc. India 76 (4), 414–418.
Piazolo, S., Passchier, C.W., 2002. Controls on lineation development in low to medium grade shear zones: a study from the Cap de Creus peninsula, NE Spain. J. Struct. Geol. 24, 25–44.
Platt, J.P., Vissers, R.L.M., 1989. Extensional collapse of thickened continental lithosphere: a working hypothesis for the Alboran Sea and Gibraltar arc. Geology 17 (6), 540–543.
Prince, C., Vance, D., Harris, N.B.W., Oberli, F., 1994. Controls on and timing of metamorphism in the Himalaya. Mineral. Mag. 62, 1210–1211.
Rajendran, K., Parameswaran, R.M., Rajendran, C.P., 2017. Seismotectonic perspectives on the Himalayan arc and contiguous areas: inferences from past and recent earthquakes. Earth Sci. Rev. 173, 1–30.
Rajendran, K., Parameswaran, R.M., Rajendran, C.P., 2018. Revisiting the 1991 Uttarkashi and the 1999 Chamoli, India, earthquakes: implications of rupture mechanisms in the central Himalaya. J. Asian Earth Sci. 162, 107–120.
Ratschbacher, L., Frisch, W., Neubauer, F., Schmid, S.M., Neugebauer, J., 1989. Extension in compressional orogenic belts: the eastern Alps. Geology 17 (5), 404–407.
Ratschbacher, L., Frisch, W., Liu, G., Chen, C., 1994. Distributed deformation in southern and western Tibet during and after the India-Asia collision. J. Geophys. Res. Solid Earth 99 (B10), 19917–19945.
Raval, U., 1995. On a Geodynamical Visualization of the Uttarkashi Earthquake and its Generalization. Memoirs-Geological Society of India, pp. 203–224.
Rey, P., Vanderhaeghe, O., Teyssier, C., 2001. Gravitational collapse of the continental crust: definition, regimes and modes. Tectonophysics 342 (3–4), 435–449.
Riaz, R., Ali, U., Li, J., Zhang, G., Alam, K., Sweetman, A.J., Jones, K.C., Malik, R.N., 2019. Assessing the level and sources of Polycyclic Aromatic Hydrocarbons (PAHs) in soil and sediments along Jhelum riverine system of Lesser Himalayan region of Pakistan. Chemosphere 216, 640–652.
Richards, A., Argles, T., Harris, N., Parrish, R., Ahmad, T., Darbyshire, F., Draganits, E., 2005. Himalayan architecture constrained by isotopic tracers from clastic sediments. Earth Planet Sci. Lett. 236 (3–4), 773–796.
Robinson, D.M., McQuarrie, N., 2012. Pulsed deformation and variable slip rates within the central Himalayan thrust belt. Lithosphere 4 (5), 449–464.
Robinson, D.M., DeCelles, P.G., Copeland, P., 2006. Tectonic evolution of the Himalayan thrust belt in western Nepal: implications for channel flow models. Geol. Soc. Am. Bull. 118 (7–8), 865–885.
Robinson, A.C., Yin, A., Manning, C.E., Harrison, T.M., Zhang, S.H., Wang, X.F., 2007. Cenozoic evolution of the eastern Pamir: implications for strain-accommodation mechanisms at the western end of the Himalayan-Tibetan orogen. Geol. Soc. Am. Bull. 119 (7–8), 882–896.
Robl, J., Stüwe, K., 2005. Continental collision with finite indenter strength: 2. European Eastern Alps. Tectonics 24 (4).
Royden, L.H., Burchfiel, B.C., King, R.W., Wang, E., Chen, Z., Shen, F., Liu, Y., 1997. Surface deformation and lower crustal flow in eastern Tibet. Science 276 (5313), 788–790.
Saha, A.K., Gupta, R.P., Arora, M.K., 2002. GIS-based landslide hazard zonation in the Bhagirathi (Ganga) valley, Himalayas. Int. J. Rem. Sens. 23 (2), 357–369.
Saklani, P.S., 1979. Folded rocks of northern Tehri garhwal Himalaya. In: Saklani, P.S. (Ed.), Structural Geology of the Himalaya, pp. 101–112.
Sarkar, S., Kanungo, D.P., Chauhan, P.K.S., 2011. Varunavat landslide disaster in Uttarkashi, garhwal Himalaya, India. Q. J. Eng. Geol. Hydrogeol. 44 (1), 17–22.
Sasvári, Á., Baharev, A., 2014. SG2PS (structural geology to postscript converter)–A graphical solution for brittle structural data evaluation and paleostress calculation. Comput. Geosci. 66, 81–93.
Saxena, S.P., 1974. Geology of the marchula-bhikiasen area, District Almora, Uttar Pradesh, with special reference to the south Almora thrust. Himal. Geol. 4, 630–647.
Scheiber, T., Viola, G., 2018. Complex bedrock fracture patterns: a multipronged approach to resolve their evolution in space and time. Tectonics 37, 1030–1062.
Schellart, W.P., Lister, G.S., Sussman, A.J., Weil, A.B., 2004. Tectonic models for the formation of arc-shaped convergent zones and backarc basins. In: Orogenic Curvature: Integrating Paleomagnetic and Structural Analyses, vol. 383. Geological Society of America, Boulder, CO, pp. 237–258.
Schmid, S.M., Berza, T., Diaconescu, V., Froitzheim, N., Fügenschuh, B., 1998. Orogen-parallel extension in the southern Carpathians. Tectonophysics 297 (1–4), 209–228.
Seeber, L., Armbruster, J.G., 1984. Some elements of continental subduction along the Himalayan front. Tectonophysics 105 (1–4), 263–278.
Seeber, L., Pêcher, A., 1998. Strain partitioning along the Himalayan arc and the Nanga Parbat antiform. Geology 26 (9), 791–794.
Sen, A., Sen, K., Srivastava, H.B., Singhal, S., Phukon, P., 2019. Age and geochemistry of the paleoproterozoic Bhatwari gneiss of garhwal lesser Himalaya, NW India: implications for the pre-himalayan magmatic history of the lesser himalayan basement rocks. Geological Society, London, Special Publications 481 (1), 319–339.
Shaanan, U., Rosenbaum, G., Pisarevsky, S., Speranza, F., 2015. Paleomagnetic data from the New England Orogen (eastern Australia) and implications for oroclinal bending. Tectonophysics 664, 182–190.
Shaikh, M., Maurya, D.M., Mukherjee, S., Vanik, N., Padmalal, A., Chamyal, L., 2020. Tectonic evolution of the intra-uplift Vigodi-Gugriana-Khirasra-Netra Fault System

in the seismically active Kachchh Rift Basin, India: implications for the western continental margin of the Indian plate. J. Struct. Geol. 140, 104124.
Shan, Y., Li, Z., Lin, G., 2004. A stress inversion procedure for automatic recognition of polyphase fault/slip data sets. J. Struct. Geol. 26 (5), 919–925.
Shanker, R., Ganesan, T.M., 1973. A note on the garhwal nappe. Himal. Geol. 3, 72–82.
Sharma, R., Bhatt, S.C., 1990. Fold wavelength: amplitude ratio in relation to thrust faults, Garhwal Himalaya, India. Tectonophysics 172 (1–2), 169–173.
Shekhar, S., Saklani, P.S., Bhola, A.M., 2006. Geology and structure of srinagar, garhwal Himalaya. Himalaya (Geological Aspects) 4, 153–169.
Simón, J.L., 2019. Forty years of paleostress analysis: has it attained maturity? J. Struct. Geol. 125, 124–133.
Singh, P., Patel, R.C., Lal, N., 2012. Plio-plistocene in-sequence thrust propagation along the main central thrust zone (Kumaon–Garhwal Himalaya, India): new thermochronological data. Tectonophysics 574, 193–203.
Sinha, R., Tandon, S.K., Gibling, M.R., Bhattacharjee, P.S., Dasgupta, A.S., 2005. Late Quaternary geology and alluvial stratigraphy of the Ganga basin. Himal. Geol. 26 (1), 223–240.
Sippel, J., Saintot, A., Heeremans, M., Scheck-Wenderoth, M., 2010. Paleostress field reconstruction in the Oslo region. Mar. Petrol. Geol. 27, 682–708.
Spang, J.H., 1972. Numerical method for dynamic analysis of calcite twin lamellae. Geol. Soc. Am. Bull. 83 (2), 467–472.
Srivastava, H.B., Cobbold, P.R., 2014. What makes India such a good indenter? Curr. Sci. 106 (2), 288.
Srivastava, P., Mitra, G., 1994. Thrust geometries and deep structure of the outer and lesser Himalaya, Kumaon and Garhwal (India): implications for evolution of the Himalayan fold and thrust belt. Tectonics 13 (1), 89–109.
Stockli, D.F., Taylor, M., Yin, A., Harrison, T.M., D'Andrea, J., Kapp, P., Ding, L., 2002. Late Miocene-Pliocene inception of EW extension in Tibet as evidenced by apatite (U-Th)/He data. Geological Society of America Abstracts with Programs 34 (6), 411.
Styron, R.H., Taylor, M.H., Murphy, M.A., 2011. Oblique convergence, arc-parallel extension, and the role of strike-slip faulting in the High Himalaya. Geosphere 7 (2), 582–596.
Takeshita, T., Yagi, K., 2004. Flow patterns during exhumation of the Sambagawa metamorphic rocks, SW Japan, caused by brittle-ductile, arc-parallel extension. Geological Society, London, Special Publications 227 (1), 279–296.
Taloor, A.K., Joshi, L.M., Kotlia, B.S., Alam, A., Kothyari, G.C., Kandregula, R.S., Singh, A.K., Dumka, R.K., 2021. Tectonic imprints of landscape evolution in the Bhilangana and Mandakini basin, Garhwal Himalaya, India: a geospatial approach. Quat. Int. 575, 21–36.
Tapponnier, P., Molnar, P., 1976. Slip-line field theory and large-scale continental tectonics. Nature 264 (5584), 319–324.
Tapponnier, P., Peltzer, G., Le Dain, A.Y., Armijo, R., Cobbold, P., 1982. Propagating extrusion tectonics in Asia: new insights from simple experiments with plasticine. Geology 10, 611–616.
Teotia, S.S., Khattri, K.N., Roy, P.K., 1999. Fractal analysis of seismicity in the Garhwal Himalayan region. In: Jain, A.K., Manickavasagam, R.M. (Eds.), Geodynamics of the NW Himalaya, vol. 6. Gondwana Research Group Memoir, pp. 341–346.
Thakur, V.C., 1992. Geology of Western Himalaya. Pergamon Press, Oxford, ISBN 0080422063, pp. 1–363.
Thakur, V.C., Kumar, S., 1994. Seismotectonics of the 20 october 1991 Uttarkashi earthquake in garhwal, Himalaya, north India. Terra. Nova 6, 90–94.
Thakur, V.C., Joshi, M., Sahoo, D., Suresh, N., Jayangondapermal, R., Singh, A., 2014. Partitioning of convergence in Northwest Sub-Himalaya: estimation of late Quaternary uplift and convergence rates across the Kangra reentrant, North India. Int. J. Earth Sci. 103, 1037–1056.
Thiede, R.C., Arrowsmith, J.R., Bookhagen, B., McWilliams, M., Sobel, E.R., Strecker, M. R., 2006. Dome Formation and extension in the tethyan Himalaya, Leo pargil, northwest India. Geol. Soc. Am. Bull. 118 (5–6), 635–650.
Treloar, P.J., Coward, M.P., 1991. Indian Plate motion and shape: constraints on the geometry of the Himalayan orogen. Tectonophysics 191 (3–4), 189–198.
Turner, F.J., 1953. Nature and dynamic interpretation of deformation lamellae in calcite of three marbles. Am. J. Sci. 251 (4), 276–298.
Turner, S.P., Kelley, S.P., VandenBerg, A.H.M., Foden, J.D., Sandiford, M., Flottmann, T., 1996. Source of the Lachlan fold belt flysch linked to convective removal of the lithospheric mantle and rapid exhumation of the Delamerian-Ross fold belt. Geology 24 (10), 941–944.
Valdiya, K.S., 1976. Himalayan transverse faults and folds and their parallelism with subsurface structures of north Indian plains. Tectonophysics 32 (3–4), 353–386.
Valdiya, K.S., 1978. Outline of the structure of KumaunHiamlaya. In: Saklani, P.S. (Ed.), Tectonic Geology of the Himalaya. Today and Tomorrow's Printers and Publishers, New Delhi, pp. 1–42.
Valdiya, K.S., 1980. Geology of Kumaun Lesser Himalaya. Wadia Institute of Himalayan Geology.
Valdiya, K.S., 1995. Proterozoic sedimentation and Pan-African geodynamic development in the Himalaya. Precambrian Res. 74 (1–2), 35–55.
Valdiya, K.S., 2010. The Making of India: Geodynamic Evolution, second ed. Springer, ISBN 978-3-319-25029-8, pp. 1–816.
Valli, F., Arnaud, N., Leloup, P.H., Sobel, E.R., Mahéo, G., Lacassin, R., Guillot, S., Li, H., Tapponnier, P., Xu, Z., 2007. Twenty million years of continuous deformation along the Karakorum fault, western Tibet: a thermochronological analysis. Tectonics 26 (4).
Valli, F., Leloup, P.H., Paquette, J.L., Arnaud, N., Li, H., Tapponnier, P., Lacassin, R., Guillot, S., Liu, D., Deloule, E., Xu, Z., 2008. New U-Th/Pb constraints on timing of shearing and long-term slip-rate on the Karakorum fault. Tectonics 27 (5).
Vanik, N., Shaikh, M.A., Mukherjee, S., Maurya, D.M., Chamyal, L.S., 2018. Post-Deccan Trap stress reorientation under transpression: evidence from fault slip analyses from SW Saurashtra, Western India. J. Geodyn. 121, 9–19.
Vannay, J.C., Grasemann, B., Rahn, M., Frank, W., Carter, A., Baudraz, V., Cosca, M., 2004. Miocene to Holocene exhumation of metamorphic crustal wedges in the NW Himalaya: evidence for tectonic extrusion coupled to fluvial erosion. Tectonics 23 (1).
Verma, R.K., Roonwal, G.S., Kamble, V.P., Dutta, U., Kumar, N., Gupta, Y., Sood, S., 1995. Seismicity of Northwestern Part of the Himalayan Arc, Delhi-Hardwar Ridge and Garhwal-Kumaon Himalaya Region: a Synthesis of Existing Data. Memoirs-Geological Society of India, pp. 83–100.
Viruete, J.E., 1999. Hornblende-bearing leucosome development during syn-orogenic crustal extension in the tormes gneiss dome, NW iberian massif, Spain. Lithos 46 (4), 751–772.
Viti, M., De Luca, J., Babbucci, D., Mantovani, E., Albarello, D., D'Onza, F., 2004. Driving mechanism of tectonic activity in the northern Apennines: quantitative insights from numerical modeling. Tectonics 23 (4).
Wadia, D.N., 1931. The syntaxis of the northwest Himalaya: its rocks, tectonics and orogeny. Record Geol. Surv. India 65 (2), 189–220.
Yin, A., 2006. Cenozoic tectonic evolution of the Himalayan orogen as constrained by along-strike variation of structural geometry, exhumation history, and foreland sedimentation. Earth Sci. Rev. 76 (1), 1–131.
Žalohar, J., Vrabec, M., 2007. Paleostress analysis of heterogeneous fault-slip data: the Gauss method. J. Struct. Geol. 29 (11), 1798–1810.
Zeng, L., Wang, H., Gong, L., Liu, B., 2010. Impacts of the tectonic stress field on natural gas migration and accumulation: a case study of the Kuqa Depression in the Tarim Basin, China. Mar. Petrol. Geol. 27, 1616–1627.
Zhang, P.Z., Shen, Z., Wang, M., Gan, W., Burgmann, R., Molnar, P., Wang, Q., Niu, Z., Sun, J., Wu, J., Hanrong, S., 2004. Continuous deformation of the Tibetan Plateau from global positioning system data. Geology 32 (9), 809–812.
Zhang, Z., Xiang, H., Dong, X., Ding, H., He, Z., 2015. Long-lived high-temperature granulite-facies metamorphism in the Eastern Himalayan orogen, south Tibet. Lithos 212, 1–15.
Zoback, M.L., Zoback, M.D., Watts, A., Schubert, G., 2009. Lithosphere stress and deformation. Crust and lithosphere dynamics 253–273. Elsevier.